SUPPORT VECTOR CLASSIFICATION ANALYSIS OF RESTING STATE FUNCTIONAL CONNECTIVITY FMRI

A Dissertation
Presented to
The Academic Faculty

By

Richard Cameron Craddock

In Partial Fulfillment
of the Requirements for the Degree
Doctor of Philosophy
in
Electrical and Computer Engineering

School of Electrical and Computer Engineering
Georgia Institute of Technology
December 2009

Copyright © 2009 by Richard Cameron Craddock

SUPPORT VECTOR CLASSIFICATION ANALYSIS OF RESTING STATE FUNCTIONAL CONNECTIVITY FMRI

Approved by:

Xiaoping P. Hu, PhD, Advisor
Professor and Georgia Research Alliance Eminent Scholar in Imaging
School of Biomedical Imaging
Georgia Institute of Technology and
Emory University

George Vachtsevanos, PhD, Co-advisor
Professor Emeritus
School of Electrical and Computer Engineering
Georgia Institute of Technology

Helen S. Mayberg, MD
Professor and Dorothy Fuqua Chair of Psychiatric Imaging and Therapeutics
Psychiatry and Neurology
Emory University

Robert Butera, PhD
Associate Professor
School of Electrical and Computer Engineering
Georgia Institute of Technology

Brian Gurbaxani, PhD
Adjunct Assistant Professor
School of Electrical and Computer Engineering
Georgia Institute of Technology
Senior Scientist
Centers for Disease Control and Prevention

Anthony Yezzi, PhD
Professor
School of Electrical and Computer Engineering
Georgia Institute of Technology

Date Approved: October 2, 2009

This dissertation is dedicated to Charles Gresham Lee and Ruby Wiggins Lee, the wells from which I draw my intelligence and strength, and to Heather Schafer, BDS (best damn sister).

ACKNOWLEDGMENTS

This dissertation represents the cap stone of a nine year graduate education that was forged at Georgia Tech, Emory University, and the CDC. I greatly apprciate the contributions of all those that have helped me acheive my PhD.

My graduate education began in the Georgia Tech School of Electrical and Computer Engineering under the tutelage of Dr. Linda Wills where I had the honor of working with Dr. Lewis Baumstark, Dr. Chris Lee, Murat Guler, and Nidhi Shah.

From the Georgia Tech and Emory University Biomedical Imaging Technology Center I would like to thank Dr. Xiaoping Hu for teaching me the foundations of fMRI. While a member of the BITC, I was mentored by Dr. Scott Peltier, Dr. Keith Heberlein, Dr. Stephen LaConte, Dr. Qin Xu, and Dr. Andy James. My education was solidified through interactions with fellow BITC students: Dr. Roger Nana, Dr. Chris Glielmi, Dr. Yang Zhe, Jaemin Shin, Steve Harris, Alex Poplawski, and Daniel Perez.

From the Emory University Department of Psychiatry I would like to thank Dr. Helen Mayberg for mentoring my development into a neuroscientist and for teaching me how to apply nueorimaging to the study of psychiatric disorders. As a member of her lab I had the honor of working with Dr. Paul Holtzheimer, Andrea Barrocas, KiSueng Choi, and Megan Filkowski; all of whom made substantial contributions to my dissertation research.

During my time spent at the Centers for Disease Control and Prevention I had the honor of working for Dr. Bill Reeves, Dr. Suzanne Vernon, Dr. Brian Gurbaxani, and Dr. Jim Jones. Of these Dr. Gurbaxani took a special interest in my education, for which I am deeply appreciative.

My long graduate career would not have been sustainable without the lifelong friends that comprise my family. I appreciate your encouragement to presevere as well as our time spent smelling the roses. Dr. Steven Kreft, Dr. Joel Hales, Ben Chen, and Chris Hart have been there since high school and have set the bar for true friendship. Their wives

Dr. Elham Kreft, Dr. Katie Hales, Nicole Chen, and Kathleen Hart have patiently endured my eccentricities. Wil and Amy Lonergan have been very good friends and supported me through the last few hurdles of my graduate career. Matt Dykes, Reed Smith, and Paul Konikowski have shown me what it is to have brothers. By no means least are those that have always been there to provide a shoulder and a distraction: Brent Harris, Gary Burpo, Jenny Burpo, Matt Tiller, Alex McIntosh, Danny Rolnick, Carrie Rolnick, Michael Waldbillig, Rebecca Loveman, and Jonathan Green.

My sister has been my guiding light since childhood. Through her accomplishments she has shown me that I can succeed. Her love and encouragement have helped me persevere those many times I wanted to quit. She has taught me that the best way to erase the past is to focus on improving the future.

I would like to thank the members of my dissertation committee for taking the time to help me over the last hurdle of my graduate career.

Last I would like to acknowledge the Georgia Tech School of Electrical and Computer Engineering, I have earned three degrees both because of you and in-spite of you.

SUMMARY

Since its discovery in 1995 resting state functional connectivity derived from functional MRI data has become a popular neuroimaging method for study psychiatric disorders. Current methods for analyzing resting state functional connectivity in disease involve thousands of univariate tests, and the specification of regions of interests to employ in the analysis. There are several drawbacks to these methods. First the mass univariate tests employed are insensitive to the information present in distributed networks of functional connectivity. Second, the null hypothesis testing employed to select functional connectivity differences between groups does not evaluate the predictive power of identified functional connectivities. Third, the specification of regions of interests is confounded by experimentor bias in terms of which regions should be modeled and experimental error in terms of the size and location of these regions of interests. The objective of this dissertation is to improve the methods for functional connectivity analysis using multivariate predictive modeling, feature selection, and whole brain parcellation. A method of applying Support vector classification (SVC) to resting state functional connectivity data was developed in the context of a neuroimaging study of depression. The interpretability of the obtained classifier was optimized using feature selection techniques that incorporate reliability information. The problem of selecting regions of interests for whole brain functional connectivity analysis was addressed by clustering whole brain functional connectivity data to parcellate the brain into contiguous functionally homogenous regions. This newly developed famework was applied to derive a classifier capable of correctly seperating the functional connectivity patterns of patients with depression from those of healthy controls.

CONTENTS

LIST OF TABLES

LIST OF FIGURES

CHAPTER 1

INTRODUCTION

The objective of this dissertation is to explore the application of support vector classification (SVC) to predict disease state from resting state functional magnetic resonance imaging (fMRI) derived functional connectivity maps (FCMs). An integral part of this exploration is applying feature selection techniques to minimize generalization error and improve the interpretation of SVC results. Additionally a data driven clustering method is developed to parcellate whole brain functional connectivity data into regions of interest (ROI) useful for whole brain functional connectivity analyses. The developed methods are then employed to identify a pattern of functional connectivity capable of distinguishing patients with depression from healthy controls. This work was performed in collaboration with the Department of Psychiatry and Behavioral Sciences, School of Medicine, Emory University.

Functional connectivity refers to correlations in physiological signals recorded from spatially distinct brain regions. Resting state functional connectivity refers to correlations in signals recorded while the subject is resting quietly and not performing a specified task. The physiological processes underlying these correlations are unknown, but it is assumed that they correspond to coherence between activity in the underlying neuronal population. Resting state functional connectivity is not novel to fMRI. It has been observed in both electroencephalography (EEG) [1, 2], positron emission tomography (PET) [3], and direct cortical recordings [4, 5], but the non-invasive nature and high spatial and temporal resolution of fMRI make it well suited for this analysis. Several recent studies have shown changes in functional connectivity for patients in pathological states including cocaine use [6], multiple sclerosis [7], Alzheimer's disease [8, 9, 10, 11], schizophrenia [12, 13, 14], attention deficit hyperactivity disorder [15], autism [16], epilepsy [17] and major depression disorder [18]. fMRI and functional connectivity are described in Chapter 2.

Individual level FCMs are typically calculated using seed-based correlation or model-free approaches such as independent component analysis (ICA). Functional connectivity differences between groups are assessed by applying mass-univariate approaches voxel-by-voxel [10, 15, 9, 13, 18]. These univariate approaches treat each voxel independently and thus are only sensitive to localized differences in connectivity. In contrast, multivariate techniques analyze all voxels simultaneously, permitting information to be accumulated between regions. This is particularly powerful in the situation where two or more voxels do not differentiate groups independently, but do so jointly. When performed in a prediction modeling framework, multivariate techniques provide a natural framework for discovering biomarkers capable of predicting disease state. SVC has become a popular multivariate method for the analysis of fMRI due to their ability to deal with small samples of high dimensional data [19, 20, 21, 22]. SVC tends to outperform other multivariate predictive modeling methods in terms of generalization error (prediction accuracy), robustness to outliers, and insensitivity to data preprocessing choices [21, 23]. Chapter 3 describes the first application of SVC to the analysis of functional connectivity in disease.

Feature selection is an important procedure to improve the performance and ease of interpretation of SVC results [24, 25, 26, 27]. Functional MRI datasets are inherently high dimensional, including many voxels that do not contain any information for the analysis being performed. Classifiers trained on these datasets will have a tendency to over-fit the data resulting in poor generalization error. Removing these meaningless voxels through feature selection reduces this tendency to over-fit. Fundamentally, the appeal of fMRI is its ability to determine the spatial pattern of brain regions involved in brain function or disease state. Feature selection reduces the input space to only those voxels most relevant to the classification or regression being performed. Thus, feature selection provides a mechanism for extracting information about the brain regions involved in the process under investigation [26, 27]. In Chapter 3 the impact of feature selection on SVC is explored and two new feature selection strategies that incorporate a reliability criterion are developed.

Feature extraction refers to the process of summarizing the input data set into a representation that is best suited for the experiment being analyzed. Indeed much of the research on applying SVC to fMRI data involves developing methods for summarizing voxel time-courses so that SVC can be applied to different experiment paradigms [19, 28, 26, 29]. For resting state functional connectivity data, the time dimension is reduced by correlation. This procedure amplifies the number of voxels to $p(p-1)/2$ (where p is the number of voxels) unique correlation coefficients. Applying SVC to datasets this large is computationally intractable even for state-of-the-art workstations. It is possible to significantly reduce the dimension of resting state fMRI data due to the substantial correlation between neighboring voxels. The challenge lies in determining how voxels should be combined so that data dimensionality is reduced without losing information. In Chapter 4 feature extract is achieved using a clustering method to parcellate whole brain resting state data into functionally homogeneous regions. In Chapter 5 the methods developed in Chapter 3 and Chapter 4 are combined to perform whole brain functional connectivity analysis of major depressive disorder. Finally, the contributions of this dissertation are reviewed in Chapter 6, the conclusion.

CHAPTER 2

RESTING STATE FUNCTIONAL CONNECTIVITY MRI

Functional connectivity is defined as "correlations between spatially remote neurophysiological events" [30]. While functional connectivity was initially studied during tasks, it has been found to exist during resting state conditions [31, 32, 33, 34]. A resting state paradigm is one in which the subject is not engaged in a specified task. The attraction of resting state analysis is that it measures brain state free of experimental confounders. The meaning of resting state is controversial and presently still under debate.

2.1 fMRI, BOLD, and the Hemodynamic Response

The most common form of fMRI derives its signal from the blood oxygen level dependent (BOLD) contrast, which was first reported by Ogawa et al[35]. Oxygen is transported in blood bound to the protein hemoglobin. At the core of hemoglobin are four atoms of iron. Hemoglobin without oxygen (deoxy-hemoglobin) is paramagnetic and results in a local magnetic field in-homogeneity that dephases the MR signal. Conversely, when oxygen is bound to hemoglobin (oxy-hemoglobin) the iron is blocked and the molecule becomes diamagnetic, which does not affect the MR signal. An fMRI time series is formed by the rapid acquisition of MR images sensitive to the BOLD effect in which regions near oxy-hemoglobin have a higher intensity then those near deoxy-hemoglobin [35].

When a region of the brain is at equilibrium, there is a constant relationship between oxy-hemoglobin and deoxy-hemoglobin; this sets the baseline for the fMRI signal. When neurons become active they consume nearby supplies of oxygen and the amount of deoxy-hemoglobin increases compared to oxy-hemoglobin, resulting in an initial dip in the fMRI signal. If the demand for oxygen persists, the flow of oxygenated blood to the activated area is increased. The rate of oxygen supplied to the region is greater than the demand and oxy-hemoglobin becomes more abundant then deoxy-hemoglobin, resulting in an increase

in the fMRI signal. After neuronal activity has ceased, the blood flow is restored to basal levels and the fMRI signal returns to baseline. This phenomenon is the hemodynamic response and characterizes the shape of the fMRI signal in an active brain region. The hemodynamic response results in a 1-5% signal change that begins 2-4 seconds after a single brief stimulus and lasts for 3-5 seconds [36].

fMRI can also be performed using techniques that measure cerebral blood flow (CBF) and cerebral blood volume (CBV). These two techniques are uncommon, and the term fMRI has become synonymous with BOLD imaging. CBF and CBV are beyond the scope of this discussion.

2.2 fMRI Experiments and Analysis

The simplest fMRI experiment utilizes a block design. The experiment is divided into probe blocks and control blocks. In the control block the subject is either at rest or performs a control task. During the probe blocks the subject performs the task of interest. These blocks are repeated several times throughout the course of an experiment, and each block generally involves multiple task trials [36]. Stimuli are presented visually using a projection device or audibly using head phones. The subjects' performance can be recorded using a button box.

The subject performs the experiment while inside an MRI scanner that is actively acquiring functional images. Each functional image consists of a series of two dimensional slices that when combined form a 3D volume of the subject's brain. The amount of brain coverage of each volume and the volume's spatial resolution dictate the temporal resolution. Typical functional imaging sequences acquire 30 4-mm thick slices, with an in-plane resolution of 3.5 mm x 3.5 mm every two seconds. Better temporal resolution can be obtained by reducing the number of slices acquired, and conversely, better spatial resolution can be obtained by increasing the amount of time between acquisitions. A high-resolution anatomical image is typically acquired during the same scanning session.

Several preprocessing steps are required for fMRI data before it can be analyzed using statistical methods. These include slice timing correction, motion correction, spatial normalization to a brain template, and spatial filtering. These are employed in task-based fMRI studies to increase the signal-to-noise ratio and to make the data directly comparable across subjects [37]. The application of different preprocessing steps, the best algorithms to implement the different preprocessing stages, and the order in which they should be applied are all under debate.

Several different methods have been proposed to analyze this type of experiment. Block design experiments can be modeled with a boxcar function that equals one during the probe conditions and zero during the control conditions (Figure 1a). This boxcar function is then convolved with a hemodynamic reference function to make it similar to the expected hemodynamic response (Figure 1b)[38]. The resulting waveform can then be correlated with every voxel. Voxels with a correlation coefficient greater than a threshold are considered active (Figure 1d). A similar univariate analysis can be performed using a general linear model that accounts for confounders such as motion and global signal [39]. Multivariate approaches have been proposed for fMRI analysis as well [40].

Typical analyses of neuroimaging data (PET, fMRI, EEG, etc.) treat brain regions as independent and test each of these regions for a significant change in signal mean between control and probe conditions. This is a segregationist view that treats the brain as a collection of independent specialized regions, each responsible for a different sub-task involved in task performance. Functional connectivity analyses on the other hand include the correlational structure between different brain regions in the analysis. This is an integrationalist view that describes the brain as several different networks in which the constituent brain regions collaborate to perform a task [30].

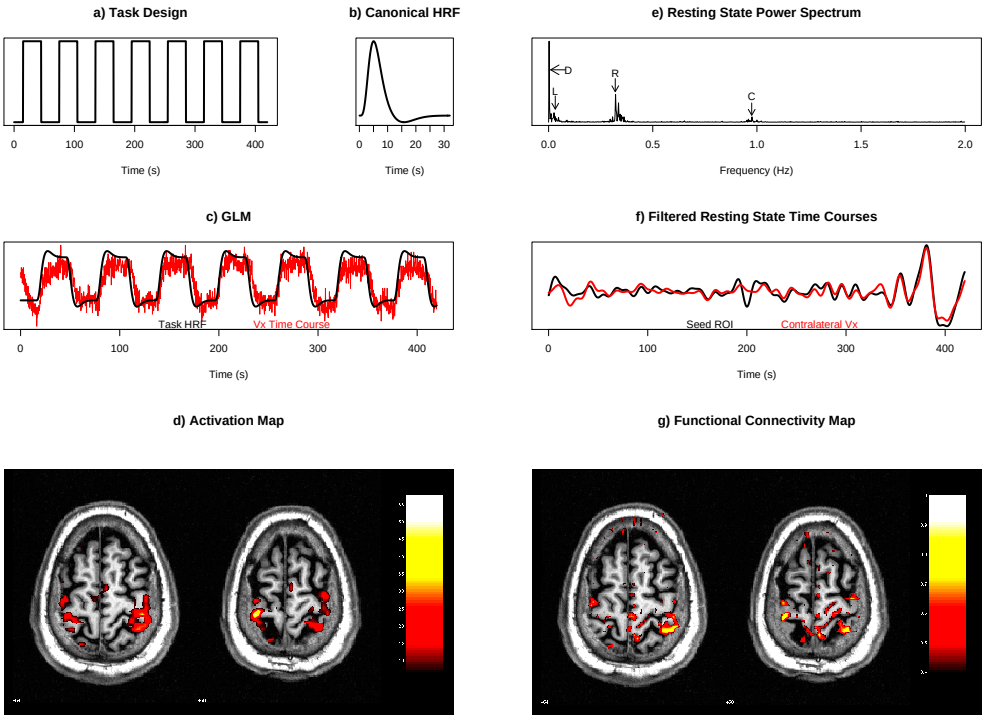

Figure 1. Example of task fMRI and functional connectivity of the motor cortices.

2.3 Resting State fMRI (rfMRI)

Fluctuations in the resting brain are observed using BOLD weighted magnetic resonance imaging [31, 41, 42, 33]. Fourier analysis of a typical time-course acquired at rest shows peaks at frequencies corresponding to pulse and respiratory rates, as well as the harmonics of these frequencies (Figure 1e). Additionally poorly characterized low frequency ($< 0.1\,Hz$) fluctuations are observed (Figure 1e) [31, 41, 42]. Biswal et al. discovered that these low-frequency fluctuations measured during rest are correlated between regions of the primary sensory motor cortex. These correlations exist both within and between hemispheres [31].

Interest in rfMRI has steadily grown since its inception. Resting state functional connectivity has been shown to exist in a number of brain networks [31, 33, 34, 32], has been revealed with data-driven analysis approaches [43, 44, 45], and has been found to be consistent across subjects [46, 44]. These fluctuations are consistent with the concept of functional connectivity defined by Friston et al. [30] and are thought to represent alterations in blood flow and oxygenation caused by spontaneous neuronal activity [47]. Several recent studies have shown changes in low-frequency correlations for patients in pathological states, including cocaine use [6], multiple sclerosis [7], Alzheimer's disease [8, 9, 10, 11], schizophrenia [12, 13, 14], attention deficit hyperactivity disorder [15], autism [16], epilepsy [17] and major depressive disorder [18]. Additionally these low-frequency correlations are modulated by anesthesia [48], prior cognitive state [49], and fatigue [50].

Functional connectivity analyses are confounded by physiological noise and gross head motion [7, 51]. Physiological noise can be removed by low-pass filtering ($< 0.08\,Hz$) the data to remove frequencies not implicated in rfMRI [33]. In order for low pass filtering to be effective, the data must be sampled fast enough that the physiological noise sources do not alias into the frequency band of interest [51]. Critical sampling is easily accomplished for respiration, but cardiac noise ($.8 - 1.5\,Hz.$ corresponding to $50 - 90\,bpm$) requires a

sampling rate of $1.6 - 3\,Hz$. This rate is unattainable for multi-slice acquisitions at typical acquisition rates ($.33 - .5\,Hz$). An alternative is to record pulse rate and respiration, fit that data to a signal model, and then remove the contribution of physiological noise from the dataset [52, 53].

Head motion is a difficult problem for functional connectivity. Gross head motion in rfMRI will cause false positives in a correlation analysis [54]; on the other hand, motion correction techniques inject spatial correlations into the data [32]. Previous rfMRI studies have used a bite bar [32] or very stringent motion thresholds ($< 0.4\,mm$) [33, 32] to control for motion. Alternatively, a method for correcting functional connectivity statistics for the spatial correlation due to motion correction can be applied [32].

2.3.1 Cross Correlation (CC) Analysis of Functional Connectivity

The first implementations of CC analysis involved simple cross correlation of a seed time-course with every other voxel in the brain [31, 32]. The adaptation of CC described herein uses a regression framework that permits confounders to be entered into the analysis [55]. Before CC can proceed, several preprocessing steps are performed to clean the data. These steps typically include motion correction, slice timing correction, spatial smoothing, and temporal filtering. Temporal filtering is an important step in CC analysis that reduces the signal to the frequency band implicated in resting state functional connectivity ($0.009\,Hz < f < 0.08\,Hz$), to remove low-frequency noise due to scanner drift, and to remove sources of high-frequency noise. Once the data is cleaned, a seed time-course is extracted from a region of interest (ROI), which can either be the time-course from a single voxel or the mean time-course for several voxels (Figure 1f). The seed time-course is compared to the time-course of every in-brain voxel using a regression model that includes the global mean time-course, residual motion parameters, physiological noise waveforms, and potentially more sources of confounding noise. The resulting β and R^2 statistics are converted into correlation coefficients to form functional connectivity maps (Figure 1g).

Several other techniques have been proposed for resting state functional connectivity

analysis such as independent component analysis (ICA) [56] and self-organizing maps [43], among others. By far the most commonly used approaches are ICA and CC.

2.3.2 Group-Level Analysis of Functional Connectivity

Before group-level analysis can proceed, each subject's data must be transformed into a standard space; this ensures that the different brains are the same size and that brain regions line up. This transform can be applied before or after the regression analysis, but is typically applied before for convenience. Single-subject correlation maps are then averaged within a single group using one sample t-tests, compared across groups using two sample t-tests, or for more complex designs, ANOVA might be performed [10, 48].

Even though many of the early studies of FC in PET were performed using multivariate analyses [30, 57, 58], these methods are rarely applied to group-level analyses of FC derived from fMRI. One exception is the seed partial least squares method originally proposed for task-based FC [59], which was later applied to resting state data [60].

CHAPTER 3

DISEASE STATE PREDICTION FROM RESTING STATE FUNCTIONAL CONNECTIVITY

The objective of this chapter is to apply SVC for the group level analysis of resting state functional connectivity and explore the impact of feature selection on this application. We introduce two new feature selection algorithms that incorporate reliability and compare them to two previously proposed feature selection strategies. We perform these evaluations in the context of a study of resting state functional connectivity in major depressive disorder (MDD). Most of this chapter has been accepted for publication in Magnetic Resonance in Medicine. It is reproduced here in accordance with that journal's copyright policy.

State-of-the-art functional connectivity (FC) analyses employ either region of interest (ROI) based correlation analysis [15] or independent components analysis (ICA) [18] to generate subject-specific functional connectivity maps (FCM) for a brain network of interest. Second level analysis proceeds by comparing FCMs between disease states, feature-by-feature, using univariate statistics. Resulting statistical maps are then subjected to null hypothesis testing to determine which features are significantly different between disease states. There are at least two drawbacks to this commonly applied method. First, the employed univariate methods, while sensitive to localized differences in FC, ignore information contained in spatially distributed patterns of FC. Second, null hypothesis testing does not provide a mechanism for evaluating the predictive power of the results.

These shortcomings can be overcome by applying multi-voxel pattern analysis (MVPA) methods [61], which have relevance for brain state prediction [19, 20, 61] and real-time fMRI applications [21]. MVPA methods are sensitive to spatially distributed information that univariate methods ignore. MVPA algorithms learn patterns from multivariate datasets that optimally differentiate observations into predetermined categories. The performance of

the learned pattern is quantified by the prediction error obtained when classifying a never-seen-before observation. This is in contrast to the strategy applied in classical univariate analyses, where the significance of features is determined by how unlikely they are to not be different between groups (null hypothesis testing). Prediction error measures how well a model matches observed data, instead of how poorly it matches the null hypothesis. This provides a natural framework for disease state prediction in which the ultimate goal is to predict the presence/absence of a disease based on observed FC.

Support vector classification (SVC) is one of the most popular MVPA methods owing to reports that it offers better prediction accuracy and is less sensitive to noise than alternative MVPA approaches [20, 21, 22, 23]. SVC using fMRI data has been applied to disease state prediction for MDD [62] and drug addiction [63] using task-based fMRI measures, ADHD using regional homogeneity (ReHo) measures derived from resting state BOLD [64], and prenatal cocaine exposure using resting state cerebral blood flow [65]. To date, SVC has not been applied to resting-state FC data for the purposes of disease state prediction.

In the context of resting-state FC, features are the correlation between two brain regions (ROIs or voxels). The number of features is $O(p^2)$ in the number of brain regions employed in the analysis. In order to reduce complexity, this preliminary analysis is performed on a set of regions previously identified in depression. A method that enables whole brain functional connectivity analysis is presented in Chapter 4 and a whole brain functional connectivity analysis is performed in Chapter 5.

Feature selection, the "process of selecting a subset of features that are useful for prediction," [66] is an important component of MVPA. Benefits of feature selection include reducing prediction error and improving the ability to interpret an MVPA model [66, 26, 27]. Filter and wrapper feature selection algorithms have been applied in fMRI analyses [20, 23, 26, 27]. Filter methods treat feature selection as a preprocessing step and remove features based on some criterion (typically univariate) independent of prediction error. Since "features that have very little discriminative power independently might be

useful when combined with other features," [66] removing features using univariate criteria, even with a very liberal threshold, is likely to remove features that are important to discrimination [27].

Wrapper methods consider feature selection as an optimization problem and select features to minimize prediction error. One such method that has been applied to fMRI is recursive feature elimination (RFE) [27]. RFE is a nested, iterative, wrapper based approach in which MVPA is trained and tested on multiple re-samplings of a dataset. After each training, feature-specific scores are calculated and the lowest scoring features are removed. This process is iterated until all features have been eliminated from the input feature space, at which point the feature set that minimizes prediction error is selected. A complication with this method lies in determining a threshold for eliminating features at each iteration. Removing too few features will result in excessive computation, and removing too many might result in the elimination of important features or the inclusion of unimportant ones [27]. Since wrapper feature selection optimizes for prediction error, it must be performed within the cross-validation (CV) to avoid biasing validation estimates [66, 21]. In each CV iteration, feature selection is performed on a different subsample of the input data. This will likely result in selecting different features each CV iteration and further confound model interpretation [23].

In an attempt to optimize the interpretation of results derived from MVPA, we introduce two alternative approaches to feature selection (one filter and one wrapper approach) that incorporate reliability. There are several benefits to incorporating reliability information into feature selection. First, eliminating features that are unreliably implicated in the discriminant will improve generalization performance of the classifier. Second, it provides a mechanism for multivariate filter feature selection. Third, eliminating unreliable features should improve the reproducibility between feature sets obtained in different replications of the experiment (or multiple CV iterations). Last it provides a less arbitrary measure for excluding features in the wrapper feature selection, and should decrease the number of

iterations required before these methods converge.

3.1 Methods

3.1.1 Support Vector Classification (SVC)

Support vector classification is derived from the statistical learning theory of Vapnik [67] to solve binary classification problems. An in-depth description of SVC can be found in Vapnik's work [67] and elsewhere [68]. A brief description is provided here. Given a set of N observations each of p input features, $\mathbf{x}_i \in \mathbb{R}^p$, with corresponding class labels $y_i \in \{-1, 1\}$, SVC attempts to define a hyperplane of the form

$$y(\mathbf{x}) = \mathbf{w}^T\mathbf{x} + b \tag{1}$$

that discriminates between the two classes. If the data are linearly separable, an infinite number of such linear hyperplanes will exist. In order to minimize generalization error, SVC chooses the unique hyperplane with the largest margin: the perpendicular distance between the decision boundary and the nearest data observations. In practice, most data are not linearly separable, and a soft-margin is introduced which allows some data points to be misclassified [67]. The hyperplane is then determined by solving the convex quadratic programming optimization problem

$$\min_{\mathbf{w}} C\sum_i \xi_i + \tfrac{1}{2}\|\mathbf{w}\|^{\mathbf{2}} \tag{2}$$

$$\text{subject to} \quad y_i(\mathbf{w}^T\mathbf{x}_i + b) \geq 1 - \xi_i \tag{3}$$

$$\xi_i \geq 0 \qquad . \tag{4}$$

In which the slack variable ξ_i is the distance of the misclassified observation from its correct side of the margin and the box constraint C controls the degree to which the misclassified data points affect the solution. Lagrange multipliers are used to simplify the constrained optimization problem in Equation 2. The result is the dual representation of the maximum margin problem in which

$$\tilde{L}(\mathbf{a}) = \sum_{i=1}^{N} a_i - \frac{1}{2} \sum_{i=1}^{N} \sum_{j=1}^{N} a_i a_j y_i y_j \langle \mathbf{x}_i, \mathbf{x}_j \rangle \tag{5}$$

is maximized with respect to **a** subject to

$$0 \leq a_i \leq C, \qquad i = 1, \ldots, N, \tag{6}$$

$$\sum_{i=1}^{N} a_i y_i = 0. \tag{7}$$

Quadratic programming is used to solve this constrained optimization problem. Once the model is trained, newly acquired functional images are classified using

$$f(\mathbf{x}) = sign\left[\sum_{i=1}^{N} a_n y_n \langle \mathbf{x}, \mathbf{x}_i \rangle + b\right]. \tag{8}$$

Based on the imposed constraints, either $a_i = 0$ or $y_i f(\mathbf{x}_i) = 1$. The observations for which $a_i \neq 0$ are called support vectors and correspond to the data-points that lie on, within, or over the margin. Thus, the discriminating hyperplane of SVC maximally separates boundary points, in contrast to Fisher's linear discriminate analysis (LDA) in which the discriminate maximally separates the class centroids.

The problem of non-linearly separable data can also be resolved by mapping the input data into a higher dimensional space, referred to as the feature space. This mapping permits the construction of non-linear classifiers in the input space without giving up the convenience of linear classifiers in the feature space. Increasing the data's dimensionality dramatically increases the computation required to compute the inner products in Equation 5 and Equation 8. The dual representation, Equation 5, requires calculation of inner products in the feature space, and not the location of the functional images in that space. Using a kernel function, provided it exists for the feature space under consideration, these inner products can be computed without mapping functional images into the feature space [67]. This substantially reduces the computational burden of calculating inner products and provides SVC with an additional tool for dealing with non-linearly separable data. The dual

representation is reformulated as

$$\tilde{L}(\mathbf{a}) = \sum_{i=1}^{N} a_i - \frac{1}{2} \sum_{i=1}^{N} \sum_{j=1}^{N} a_i a_j y_i y_j k(\mathbf{x}_i, \mathbf{x}_j) \tag{9}$$

where $k(x_i, x_j)$ is the kernel function. Prediction is accomplished by

$$\hat{y}(\mathbf{x}) = sign \left[\sum_{i=1}^{N} a_i y_i k(\mathbf{x}, \mathbf{x}_i) + b \right]. \tag{10}$$

Some examples of kernel functions are listed in Table 1.

Table 1. Examples of kernel functions.

Name	Kernel	Dimension
Linear	$\langle \mathbf{x}_i, \mathbf{x}_j \rangle$	1
Quadratic	$\langle \mathbf{x}_i, \mathbf{x}_j \rangle^2$	2
Polynomial	$\langle \mathbf{x}_i, \mathbf{x}_j \rangle^d$	d
Gaussian Radial Basis Function	$e^{-\gamma \|\mathbf{x}_i - \mathbf{x}_j\|^2}, \gamma > 0$	∞

SVC is not effective at obtaining good prediction accuracy unless it is tuned using model selection and feature selection. The performance of SVC is determined using model validation. These important steps are described below.

3.1.1.1 Model Selection

Model selection is the process in which parameters are selected to optimize model performance (minimize prediction error). This is performed in cross-validation were the dataset is iteratively split into training and test datasets. A SVC model is learned from the training data and applied to classify the testing data. Misclassification error is measured as:

$$L(\mathbf{X}_{train}, \mathbf{X}_{test}) = \frac{1}{|\mathbf{X}_{test}|} \sum_{j \in \mathbf{X}_{test}} I(y_j \neq y_j^*), \tag{11}$$

where $\mathbf{X}_{test}$ is the test set, $y_j$is the true label and y_j^* is the label predicted by the model trained on $\mathbf{X}_{train}$, the training dataset, for the j^{th} sample, and $I(\theta)$ is the indicator function which equals one when is θ true and zero otherwise. In other words, misclassification error is ratio of the number of misclassified test samples to the total number of test samples.

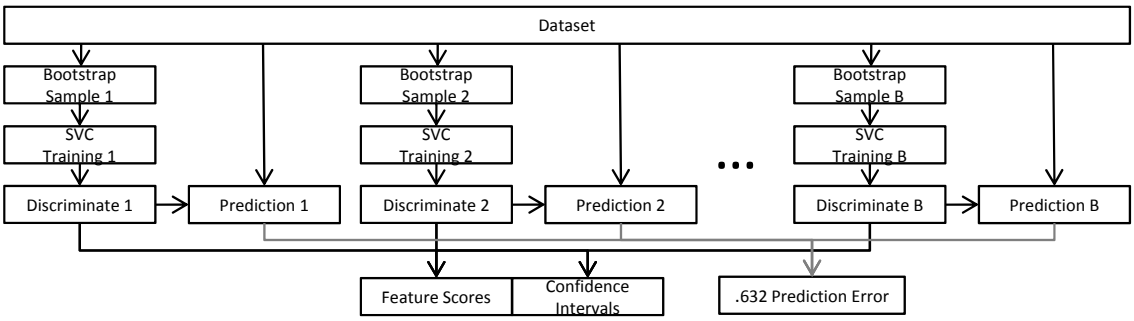

Figure 2. The bootstrap procedure.

Several options exist for estimating prediction error, we chose the .632 bootstrap method since it has low bias and variance compared to other methods [69]. The bootstrap estimator is also used to estimate feature-specific scores and confidence intervals.

The bootstrap is illustrated in Figure 2. B bootstrap samples are generated by drawing N (N = # of observations) observations from the original dataset with replacement. In each bootstrap sample some observations will be left-out and others will be duplicated. SVC is trained on the bootstrap sample and the resulting model is used to calculate prediction error, feature-specific confidence intervals, and feature-specific scores.

Prediction error is calculated by using the model learned from the bootstrap sample to predict the labels of the original dataset. Since on average .632 of the samples will be shared between the training and test set; this prediction error estimate will be biased. This is corrected using a weighted average of the prediction error calculated on the entire original sample and that calculated solely on the samples left-out of the bootstrap sample;

$$Err^{.632} = .368 * (\frac{1}{B}\sum_{b=1}^{B} L(\mathbf{X}_b, \mathbf{X})) + .632 * \frac{1}{N}\sum_{j=1}^{N}\frac{1}{|C_{j-}|}\sum_{b\in C_{j-}} L(\mathbf{X}_b, \mathbf{x}_j), \qquad (12)$$

where $\mathbf{X}$ is the original dataset, $\mathbf{X}_b$ is the b^{th} bootstrap dataset, and C_{j-} is the set of bootstrap datasets that do not include the j^{th} observation.

The discriminate will not change if only non-SVs are left out of the bootstrap sample. Because of this, we only use bootstrap samples that exclude at least one SV. This should provide a conservative estimate of CIs, feature scores and prediction error.

3.1.1.2 Feature Selection

In this work, we introduce two new feature selection approaches: reliability filter (RF) and reliability reverse feature elimination (RRFE). These are compared with two commonly used approaches: t-test filter (TF) [28], and standard recursive feature elimination (RFE) [27]. These methods are developed and compared in the context of both linear and non-linear SVC.

T-test filter (TF) TF is performed by first calculating feature-wise t-tests to determine features that have different group means. Features passing a liberal statistical threshold ($p < 0.05$, uncorrected) are retained for (linear or non-linear) SVC analysis.

Recursive feature elimination (RFE) RFE is a wrapper feature selection procedure in which the feature set is optimized by minimizing prediction error (Figure 3 excluding box). In each RFE iteration, prediction error is estimated for the current feature set along with a score for each feature using the .632 bootstrap procedure described previously. Feature specific scores are calculated by averaging the separating hyperplane calculated on each bootstrap sample

$$FS_i = \frac{1}{B}\sum_{b=1}^{B}|w_{ib}|, \tag{13}$$

where $\mathbf{w}_{ib}$ is the weight corresponding to the i^{th} feature of the hyper-plane $\mathbf{w}$ learned from the b^{th} bootstrap sample. For non-linear kernels w_{ib} is unknowable but $|w_{ib}|$ can be calculated from

$$|w_{ib}| = \sqrt{\sum_{c\in C_b}\sum_{d\in C_b} a_c y_c a_d y_d k(x_{ic}, x_{id})}, \tag{14}$$

where $C_b$is the set of observations in the b^{th} bootstrap sample.

The feature scores are used to rank the features, the lowest 20% are excluded, and the .632 bootstrap procedure is repeated to estimate prediction error and feature scores for the reduced dataset. This procedure is repeated until all features have been exhausted, at which time the feature set with the best prediction accuracy is retained for future analysis.

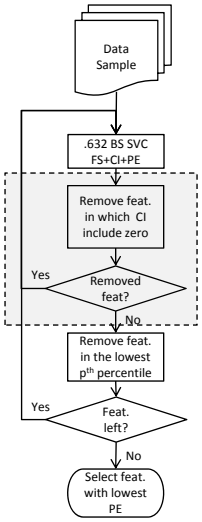

Figure 3. (Reliability) Recursive Feature Elimination

Reliability filter (RF) RF is a multivariate approach that retains features most reliably implicated in the discriminating hyperplane. This is an adaptation of a previously described approach for determining a threshold for multivariate patterns derived from partial least squares [58]. For linear SVC, bootstrap confidence intervals are derived for each feature by aggregating the hyper-planes calculated across all bootstrap samples and using the α and $1-\alpha$ percentile feature weights as the lower and upper confidence intervals respectively [69]. This approach was chosen since it doesn't require any assumptions about the distribution of w_i. Once the bootstrap confidence intervals are estimated, features whose $(1-\alpha)\%$ confidence intervals include zero are excluded from future analysis.

For nonlinear kernels, Equation 14 is employed to estimate a bootstrap distribution of $|w_i|$. This results in a folded distribution and confidence intervals cannot be directly estimated from the percentiles or standard error of this distribution. If w_i follows a normal distribution then $|w_i|$ will follow a folded normal distribution [70] described by the density function:

$$f(x) = \frac{1}{\sigma\sqrt{2\pi}}\left[e^{-(x-\mu)^2/2\sigma^2} + e^{-(x+\mu)^2/2\sigma^2}\right], x \geq 0. \tag{15}$$

The standard deviation, $\hat{\sigma}$, and the mean, $\hat{\mu}$, of the folded normal distribution can be estimated from the second and fourth moments of the bootstrap distribution of $|w_i|$ [70]. The second, m'_2, and fourth, m'_4, moments of the folded distribution of $|w_i|$ are calculated by:

$$m'_r = \frac{1}{B}\sum_{b=1}^{B} |w_{ib}|^r. \tag{16}$$

The standard deviation and mean are then determined by solving the system of equations:

$$\frac{m'_4}{(m'_2)^2} = \frac{3+6\theta^2+\theta^4}{(1+\theta^2)^2}, \tag{17}$$

$$\hat{\sigma}_i = \sqrt{\frac{m'_2}{\theta}}, \tag{18}$$

$$\hat{\mu}_i = \theta\hat{\sigma}_i. \tag{19}$$

The i^{th} features is excluded if

$$\frac{|\hat{\mu}_i|}{\hat{\sigma}_i} > \varphi^{-1}(1-\frac{\alpha}{2}), \tag{20}$$

where φ^{-1} is the inverse standard normal distribution function.

Reliability recursive feature elimination (RRFE) RRFE is very similar to the RFE approach except that it uses bootstrap confidence intervals to remove unreliable features (Figure 3 including box). If no unreliable features are identified, RRFE defaults to RFE and removes features that rank in the lowest 20%. After the features have been exhausted, the feature set that maximizes prediction accuracy is retained for further analysis.

3.1.1.3 Model Validation

Leave-one-out cross-validation (LOOCV) is performed to estimate the generalizability of the trained SVC (Figure 4). Filter feature selection can be performed before cross-validation without biasing the estimated prediction error. Wrapper methods, since they optimize for prediction error, must be performed in the cross-validation procedure. The location of these two feature selection schemes are illustrated by the gray boxes in Figure 4.

In each iteration of the cross-validation procedure, one of the observations is chosen as the test data and the remaining observations are used for training. SVC is trained on

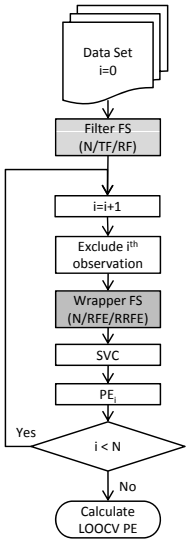

Figure 4. Leave-one-out cross-validation procedure

the training data and wrapper feature selection (if specified) is performed. Misclassification rate (11) is calculated using the classifier to predict class membership of the left-out observation. Classification performance is averaged over the N iterations of the LOOCV procedure to estimate prediction error.

3.1.2 Subjects

Forty subjects were recruited in accordance with Emory University Institutional Review Board policy. Twenty subjects (MDD; 12 F, mean age 43.2 +/- 10.8) met DSM IV criteria for a current major depressive episode without any co-morbid psychiatric disorders and had a minimum 17-item Hamilton Depression Rating Scale score of 20 (mean 23.7 +/- 1.6) at the time of scanning. Twenty healthy controls (HC; 12F, mean age 28.9 +/- 7.2) with no history of major depression were recruited for comparison; controls had a maximum Zung Self-Rating Depression scale score of 45 (mean 34.6 +/- 4.4) at the time of scanning. To qualify for inclusion subjects were required to be between the ages of 18 to 65, have no contraindications for MRI procedures, to be medication free, and without history of current or past neurological or psychiatric conditions.

3.1.3 Scanning

All subjects were scanned at the same facility on a 3.0T Siemens Magnetom TIM Trio scanner (Siemens Medical Solutions USA; Malvern PA, USA). All HC subjects were scanned with a circularly polarized transmit-receive head coil. Anatomic images were acquired at 1x1x1 mm^3 resolution with an MPRAGE sequence using the following parameters: FOV 224x256x176 mm^3, TR 2600 msec, TE 3.02 msec, FA 8°. Functional data were acquired with a Z-SAGA sequence to minimize susceptibility artifacts [71]. Two hundred and ten functional volumes were acquired in twenty 4-mm axial slices using the parameters: TR 2020 ms, TE1/TE2 30 ms/66 ms, FA 90°, in-plane resolution 3.44x3.44 mm^2. The twenty MDD subjects were scanned with a 12 channel head matrix. Anatomic images were acquired at 1x1x1 mm3 resolution with an MPRAGE sequence using: FOV 224x256x176 mm^3, TR 2600 ms, TE 3.02 ms, FA 8°, GRAPPA factor 2. Functional volumes were acquired with the same sequence and scanning parameters as HC.

For resting state functional scans subjects were instructed to passively view a fixation cross while "clearing their minds of any specific thoughts." The fixation cross was used to discourage eye movement and help prevent subjects from falling asleep. Compliance was assessed during an exit interview; all subjects confirmed they had performed the task as requested without falling asleep.

3.1.4 Preprocessing

All preprocessing of MRI data was performed using SPM5 [39] running in MATLAB 2008a (The Mathworks; Natick MA, USA). Anatomic and fMRI data were evaluated for imaging artifacts such as excessive ghosting, banding, and other imaging errors. No images had to be removed. Anatomic scans were simultaneously segmented into white matter (WM), gray matter (GM), and cerebral-spinal fluid (CSF) and normalized to the ICBM462 normalized brain atlas. fMRI volumes were slice timing corrected, motion corrected, written into ICBM462 space at 4x4x4 mm^3 resolution using the transformation calculated on the corresponding anatomic images and spatially smoothed using a 6-mm

FWHM Gaussian kernel. No images had to be removed due to excessive head motion (max motion < 2.15 mm, mean .88 mm +/- .52). De-noising of fMRI time-courses was accomplished by regressing out motion parameters, global mean time-course, WM time-course, as well as CSF time-course [55, 72]. Each voxel time-course was band-pass filtered ($0.009Hz < f < 0.08Hz$) to remove frequencies not implicated in resting state functional connectivity [33, 55].

3.1.5 ROI Selection and Time Course Extraction

ROI mask generation and time-course extraction was performed using the AFNI tool-set (Cox 1996; Cox and Hyde 1997). Fifteen in-brain ROIs were selected based on their relevance to MDD [73] (see Table 2). ROIs were constructed by a clinically trained neuroanatomist (HSM) as 6-mm radius spheres using the anatomy of the ICBM462 brain anatomic template. Lateralized ROIs were chosen in the right hemisphere.

Table 2. ROI names and coordinates

ROI	MNI (RAI)	ROI	MNI (RAI)
subcollosal cingulate cortex (scACC25)	0,-24,-12	hippocampus	-30, 24, -13
amygdala	-22, 7, -17	ventral posterior cingulate cortex (vPCC)	0, 50, 24
mid-cingulate cortex (MCC24)	0, -24, 21	dorsomedial prefrontal cortex (dMF10)	0, -62, 14
orbitofrontal cortex (OF11)	0, -49 -10	dorsolateral prefrontal cortex (dlPFC9)	-35, -49, 25
rostral anterior cingulate cortex (rACC24)	-4, -40, 0	anterior insula	-43, -14, 8
nucleus accumbens	-15, -7, -12	hypothalamus	-7, 9, -4
subgenual cingulate (sgACC24|25)	-4, -33, -9	ventral medial prefrontal cortex (vMF10)	-4, -66, 1
dorsomedial thalamus	-7, 13, 10		

Time course extraction was performed by first sub-sampling the ROI mask to match the resolution of the functional scans. For each subject, ROIs were restricted to gray matter

using the subject's gray matter mask. Time-courses were extracted from every voxel in a ROI and reduced to the first eigenvariate from singular value decomposition [74]. This procedure was performed for every region in the ROI mask, resulting in fifteen time-courses per subject.

3.1.6 SVC of Functional Connectivity

SVC of functional connectivity was performed using custom scripts running in MATLAB using the SVC functions from the Bioinformatics Toolbox. All unique pairwise correlations of ROI time-courses were calculated for each subject resulting in 105 correlation coefficients per subject. Correlation coefficients were converted to z-scores using the Fisher transform. The resulting correlation maps can be reduced using a feature selection filter. These data were entered into a support vector classification (SVC) analysis to discriminate MDD from HC. The box constant was set to 1,000,000 (hard margin) following previous observations that this is sufficient for fMRI data [21, 23]. Leave-one-out cross-validation (LOOCV) was performed to estimate the generalizability of the trained SVC. This procedure was performed ten times – once for each combination none, TF, RF, RFE and RRFE feature selection strategies and linear and quadratic kernels.

RF, RFE, and RRFE feature selections used the 1,000 iterations of the bootstrap procedure to estimate prediction error, feature-specific confidence intervals, and feature-specific scores. 95% confidence intervals were used for RF and RRFE. The TF and RF strategies were applied to the entire dataset prior to the LOOCV procedure. Since RFE and RRFE optimize prediction error, they must be performed during cross-validation. This is likely to result in different subsets of features selected each iteration of the CV procedure. The reproducibility of a feature's selection across CV iterations was evaluated by Fleiss' kappa coefficient [75].

The resulting model discriminants calculated when using RF and TF are averaged across the N iterations of the LOOCV procedure and are transformed into FCMs for visualization. The weight corresponding to each feature in the map is the relative importance

of this feature to the calculated discriminate. For the RFE and RRFE the percentage of time that a feature was called across the iterations of CV are calculated and displayed as a FCM. This percentage is negative if the feature has a negative weight and positive for a positive weight (i.e., -1 indicates that the feature survives feature selection, and has a negative weight, in all of the CV iterations).

3.2 Results

Linear support vector classification was able to distinguish MDD from HC 95% of the time using the best feature selection method of the four tested. Even in the case of no feature selection, linear SVC was able to correctly predict a subject's disease state (depressed or healthy control) with 62.5% accuracy (Table 3). The quadratic kernel performed worse than the linear kernel for all feature selection strategies except for TF, and performed better than linear when no feature selection was employed. A t-test analysis using a FDR controlled $p<0.05$ did not identify any differences between groups (Figure 6).

Table 3. Results of SVC analyses

Feature Selection	Kernel	LOOCV	# Features	# SVs	Fleiss' Kappa	Iterations
RF	linear	5.0%	11.0	10.8	1.00	1.0
RF	quadratic	20.0%	14.0	19.9	1.00	1.0
RRFE	linear	15.0%	9.8	9.4	0.77	7.9
RRFE	quadratic	32.5%	12.9	18.7	0.75	4.3
TF	linear	17.5%	11.0	10.3	1.00	1.0
TF	quadratic	12.5%	11.0	15.7	1.00	1.0
RFE	linear	37.5%	16.1	13.5	0.54	20.0
RFE	quadratic	40.0%	10.4	17.6	0.58	20.0
None	linear	37.5%	105.0	30.0	1.00	1.0
None	quadratic	27.5%	105.0	36.1	1.00	1.0

As expected, each of the tested feature selection methods improved or matched the

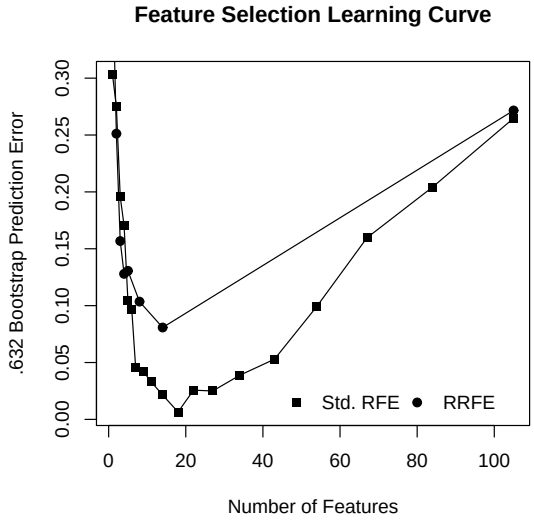

Figure 5. Feature selection learning curves produced by the RFE and RRFE feature selection methods and linear SVC.

LOOCV prediction error of SVC without feature selection, except for RFE with a quadratic kernel. The impact of feature selection on linear SVC performance is illustrated using learning curves derived from RFE and RRFE (Figure 5). With all 105 features, SVC over-fits the data, and high prediction error is observed. Prediction error decreases as features are removed until an optimum feature subset is reached which minimizes prediction error. Removing additional features under-fits the model and prediction error increases.

Standard recursive feature elimination did not improve the performance of SVC for either kernel, and was the worst of the feature selection methods compared. This lackluster performance is likely due to the large number of inconsistent features selected by this method (Figure 6d and Figure 7d). In fact, if all of the inconsistent features were removed from the RFE feature maps, the results would be similar to the features chosen by RF, the best performing method.

The performance of standard recursive feature elimination was dramatically improved by incorporating information about feature reliability. This improvement is at least in part attributable to a reduction in the number of inconsistently selected features (Figure 6e and Figure 7e). Based on Fleiss' kappa statistic the results of RRFE are substantially more

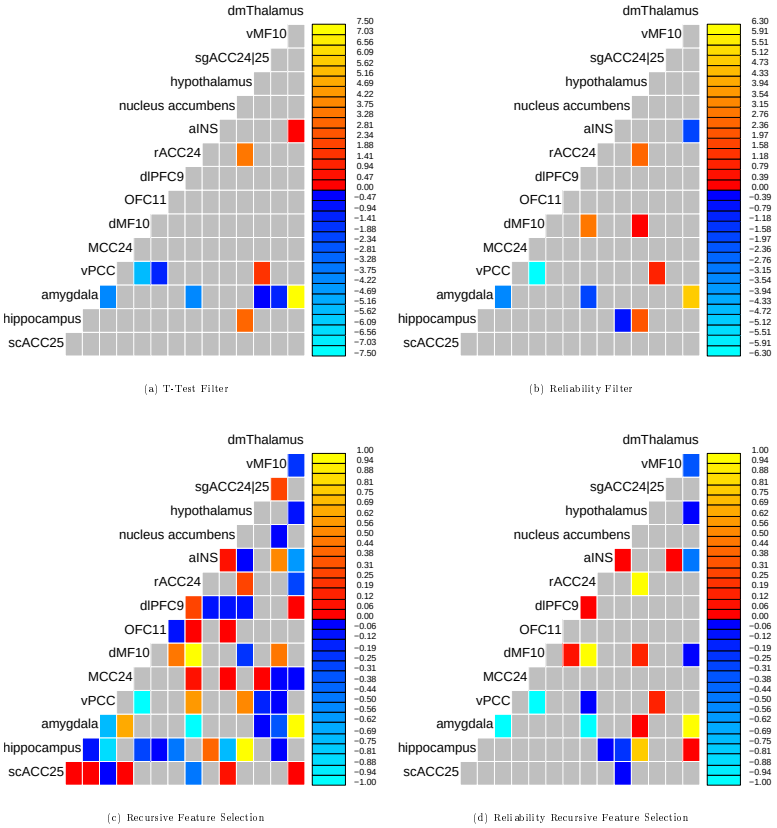

(a) T-Test Filter (b) Reliability Filter

(c) Recursive Feature Selection (d) Reliability Recursive Feature Selection

Figure 6. Discriminate maps generated from four different feature selection algorithms and linear SVC.

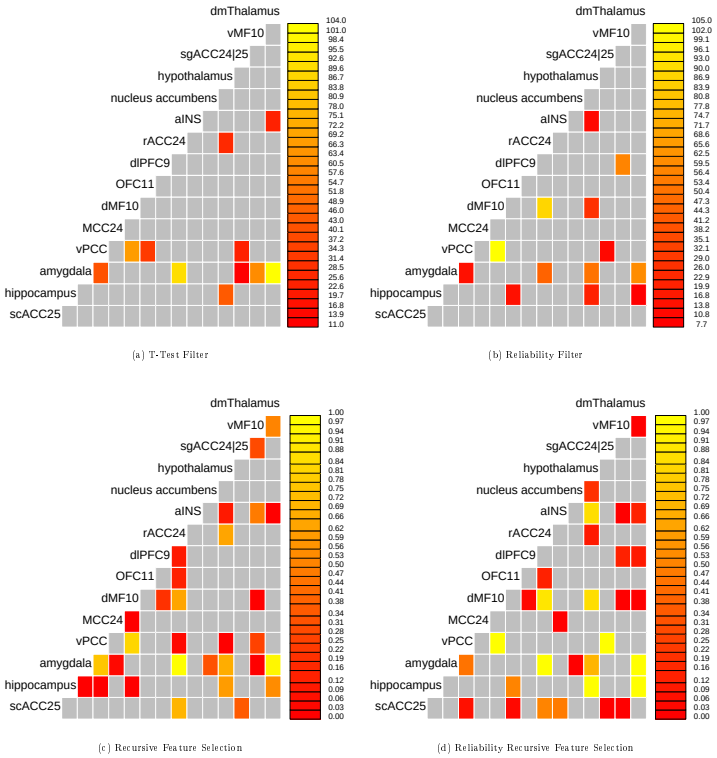

Figure 7. Discriminate maps generated from four different feature selection algorithms and quadratic SVC.

reproducible across CV iterations than RFE (Table 3). The RRFE algorithm is able to exhaustively search the feature space in less than half the number of iterations of RFE (Table 3). This is further illustrated in Figure 5 where RRFE removes over 80% of the features in its first iteration; in comparison it takes RFE nine iterations to remove the same amount.

T-test filtering was employed using feature-wise t-tests and a liberal threshold: $p < 0.05$ uncorrected. Contrary to our expectations, TF with the linear kernel performed significantly better than RFE, and only slightly worse than the proposed reliability-based multivariate methods. TF performed the best for the quadratic kernel. Investigation of the selected features (Figure 6a) shows that linear TF selected 8 out of the 11 features that linear RF selected and 3 additional features to linear RF.

The reliability filter method achieved 95% LOOCV with the linear kernel. It selected all of the most consistent features of the other techniques (Figure 6). The eleven features implicated by RF are explored in detail in Figure 8. None of the features would have been identified using a t-test and multiple comparison correction. RF was the second best with the quadratic kernel, significantly worse than TF.

There is a significant difference in age ($p < .0001$) and in head coil used for scanning between the MDD and HC groups. In order to investigate the impact of these differences on classification, six additional depressed patients meeting DSM IV criteria for a current major depressive episode without any co-morbid psychiatric disorders (6F, mean age 26.4 +/- 3.1) and scanned with the same head coil and scanning procedures as HC, were used for a hold out validation procedure.

After the previously described SVC procedure was performed for each feature selection algorithm (none, TF, RF, RFE, and RRFE) and kernel (linear, quadratic) hold-out validation was performed. An additional SVC training was performed using all of the MDD and HC samples as the training dataset and the MDD hold-out group (MDD-HO) as the testing dataset and the features retained by the feature selection procedure. For RFE and RRFE,

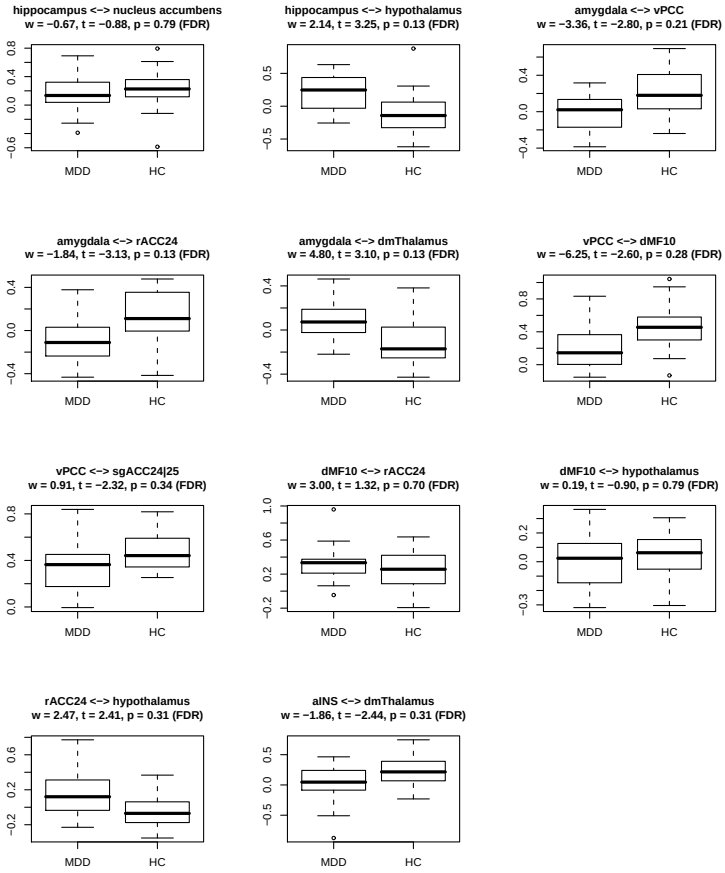

Figure 8. Features implicated by reliability filter feature selection with linear SVC.

Table 4. Results of Hold-out Validation

Feature Selection	Kernel	Hold-out Error
RF	linear	16.67%
RF	quadratic	33.33%
RRFE	linear	16.67%
RRFE	quadratic	33.33%
TF	linear	33.33%
TF	quadratic	33.33%
RFE	linear	50%
RFE	quadratic	16.67%
None	linear	83.33%
None	quadratic	50%

which select a different feature set for each iteration of LOOCV, features that were chosen in at least 50% of the LOOCV iterations were retained. The results of this procedure are listed in Table 4.

Without feature selection, hold-out error is high and only one of the six hold-out subjects is correctly identified with the linear kernel. Hold-out error is dramatically improved with feature selection and the two reliability based feature selection algorithms performed the best. For linear SVC, the ranking of feature selection algorithms based on hold-out error is the same as that obtained with LOOCV. Quadratic SVC has worse hold-out error than linear SVC for all but RFE and no feature selection.

3.3 Discussion

This study illustrates the potential utility of resting functional connectivity as a biomarker of disease. Functional connectivity patterns defined using linear support vector classification are able to predict whether a subject is a healthy control or a clinically depressed

patient at least 62.5% and as much as 95% of the time, depending on the feature selection method employed. This is substantially better than the 50% accuracy that would be achieved by chance on the same dataset. A t-test analysis ($p<0.05$ FDR corrected) performed on the same data found none of the features implicated by the most generalizable (least prediction error) SVC method employed. Using a more liberal threshold ($p<0.05$), t-tests find eleven features, eight of which overlap with those identified by the RF method. The most important feature for discriminating MDD from HC as determined by SVC was not found by either t-test analysis. Thus, SVC is more sensitive than t-tests for finding functional connectivity patterns that differentiate MDD from HC, and likely disease states in general. The three features that were identified by TF and not by RF were excluded by RF due to poor reliability.

The performance of SVC varies based on feature selection method and kernel employed. Recursive feature elimination was previously applied to fMRI analysis [27]. In that study RFE outperformed the univariate filter methods to which it was compared. The results presented here contradict that finding. A univariate t-test filter outperforms RFE by a factor of two. Possible reasons for the discrepancy are that the previous study [27] applied feature selection to a dataset with much higher dimensionality. We attribute poor performance of RFE in our study to the large number of unreproducible features that it selects. To resolve this issue, we propose an improvement to RFE that incorporates an estimate of feature reliability into the feature selection criterion.

The RRFE technique achieves better prediction accuracy than RFE (Table 3). A qualitative comparison of the results generated by the two techniques indicates that RRFE is successful in reducing the number of unreproducible features selected (Figure 6 c vs. d and Figure 7 c vs. d). This observation is confirmed by a comparison of Fleiss' kappa statistics calculated on the feature sets selected by each technique across iterations of cross-validation (Table 3). While the method we used to calculate Fleiss' kappa is biased, since

the data sets on which the compared results were generated are not independent, it is sufficient for this comparison. A split-half resampling approach is required to determine the true reproducibility obtainable by the techniques (see, e.g., [76, 23]).

Additionally, the reliability criterion used in RRFE results in a much quicker examination of the feature space than RFE (Figure 5). This reduction in the number of iterations required for feature elimination does not directly translate into reduced computational time, however. Estimating bootstrap confidence intervals requires more iterations than what is required for estimating prediction error. Nevertheless, a less arbitrary measure for eliminating features is a substantial improvement to RFE.

With a linear kernel, the TF univariate feature selection method outperforms RFE and performs worse than the proposed RRFE and RF multivariate methods. This is likely due to the insensitivity of the t-test to the dMF10 <-> rACC24 and dMF10 <-> hypothalamus connectivity. These features were found to be highly relevant to discriminating MDD from HC in all three of the multivariate feature selection methods employed. However, this illustrates a fundamental aspect of univariate feature selection that may limit its utility: univariate feature selection reduces the feature set to those features that discriminate in a univariate sense, thus removing features that can only be identified using multivariate methods. Thus, while univariate feature selection performed reasonably well in discriminating MDD from HC in our sample, it did not identify the most relevant feature for classification – thus requiring the use of a multivariate feature selection algorithm.

Based on our findings, we introduce a multivariate filter method (RF) for feature selection. Instead of using prediction error to select features, RF uses feature-specific confidence intervals estimated from multiple retraining of SVC on different subsamples of the input data. Our implementation of RF outperforms all of the other feature selection methods studied and achieves 95% prediction accuracy with the linear kernel.

The improved performance of RF over RRFE is unexpected particularly since RRFE explicitly optimizes for prediction error. Each iteration of RRFE includes the RF procedure,

but since it is performed inside CV, reliability is estimated from fewer samples than in RF. This may be one reason for the discrepancies in performance. If the sample sizes were the same, the results of the first iteration of RRFE would reduce the features to the exact same feature set as RF. Indeed the features selected by RF are the most consistently identified in RRFE. Additionally the computational cost of RF is much less than RFE or RRFE since it is performed outside of the cross-validation procedure.

Quadratic SVC outperforms linear SVC in the two cases when the same features are used for both kernels (TF and no feature selection). This is expected since the quadratic kernel has more options available for discriminating observations. The linear kernel performs better when SVC information is utilized to optimize the feature set. It may be that imposing linear separability results in a more stringent criteria for feature selection.

The high prediction accuracy (low LOOCV error) obtained might be due to age differences or head coil differences between MDD and HC groups. We investigate this using six additional depressed subjects with similar age range and scanned with the same scanning procedure as the healthy controls. SVC without feature selection had the worse hold-out prediction error, much worse than what would be expected by chance. This further illustrates SVC's tendency to over-fit when no feature selection is employed. All of the feature selection algorithms improved the hold-out prediction error, with RF and RRFE have the best performance; correctly predicting the disease states in five of the six subjects. This provides some evidence that the prediction accuracy of RF and RRFE are not confounded by the imaging coil or age. The analysis performed on this admittedly suboptimal dataset, nevertheless, illustrates the ability of SVC to learn a classifier to distinguish groups, the importance of feature selection for optimizing prediction accuracy, and the superiority of the proposed reliability based feature selection methods over t-test filter and recursive feature elimination.

3.4 Conclusion

We successfully applied support vector classification to identify a pattern of resting state functional connectivity that accurately predicts whether a subject suffers from MDD. To improve SVC performance, we introduced two feature selection algorithms that incorporate reliability information, illustrate their use with both linear and non-linear SVC, and evaluated these against two methods previously used for fMRI analysis. Our feature selection methods out-performed the previous methods in terms of prediction error as well as reproducibility of results. The proposed framework for applying SVC to functional connectivity data is applicable to other disease states beyond major depression.

CHAPTER 4

DEFINING ROIS BY CLUSTERING RESTING STATE FMRI DATA

The objective of this chapter is to develop a feature extraction method to reduce the dimensionality of whole brain resting state fMRI data. The purpose is to segregate the brain data into regions of interests (ROIs) suitable for whole brain functional connectivity analysis. The majority of this chapter has been submitted for publication and is currently under review.

When investigating the role of functional connectivity in disease, it is first necessary to define the functionally distinct brain regions to be analyzed or modeled. A simpler, alternative approach would be to use a whole-brain voxel-wise analysis, but such an approach would be computationally expensive, sensitive to noise, and difficult to interpret. Additionally, much redundant information is present at the voxel scale, as most neuroimaging studies assume that functional units of the brain are much larger than a single voxel. But as with all data-reduction approaches, the optimal means by which to combine voxels into functionally distinct regions of interest (ROIs) remains to be determined.

One approach is to manually define ROIs using anatomical images or templates, which requires hypothesizing the shape, size, and location of functional areas based upon neuroanatomic literature. This is a laborious process, prone to experimenter bias and error. These issues can be overcome using standardized ROI atlases developed from anatomical [77] or cyto-architectonic [78] boundaries. Unfortunately, neither of these approaches incorporates information about functional specialization, and both likely result in ROIs that encompass functionally heterogeneous areas. Indeed, it has been shown that adjacent regions of the anterior cingulate cortex (ACC) have drastically different structural [79] and functional connectivity patterns [80] even though the ACC is typically represented as a single ROI in brain atlases [77]. Also, small world network analysis has shown that small

world network statistics varies significantly based on the ROI atlas used [81]. To circumvent these issues, we introduce a data-driven approach for deriving functionally homogeneous ROIs from resting state functional connectivity data.

Data driven parcellation (or clustering) of functional data is not a new concept. Several approaches have been proposed for clustering task based and resting state data (e.g. independent components analysis [82], self-organizing maps [43], normalized-cut spectral clustering [83], K-means [84], and hierarchical clustering [85]). These methods focus on identifying functional networks rather than spatially distinct functional regions. However, the synchronicity of activity between distinct brain regions can vary dramatically depending upon the sensory or cognitive task being performed [86]. Therefore, functional brain patterns captured by these network-based approaches are incomplete and arguably inadequate. Neuroimaging methodology would benefit greatly from an atlas of functionally distinct brain regions which could then be implemented in network analyses.

Several approaches have attempted to develop such an atlas. Patel et al. identified anatomically distinct ROIs, then subdivided them into functionally homogeneous regions using an hierarchical clustering approach [87]. Their approach relies upon anatomic priors. Bellec et al. proposed a region growing method to identify functionally homogeneous regions in individuals [45]; that method is not appropriate for group-level clustering. Lastly, Cohen et al. proposed an edge detection method to identify functionally homogeneous areas within regions of cortex [88], but the approach is too computationally intensive to be practical for whole brain analysis. We extend this research by developing a data driven method for clustering whole brain functional connectivity data into contiguous regions without incorporating anatomical information. This method can be performed at the individual subject and group level.

Parcellating functional data can be performed for two main goals. The first is to reduce functional data to a computationally tractable size while preserving its structure. The second is to better understand functional neuroanatomy by identifying the number, size and

shape of functional units in the brain (e.g., [88]). While we believe the present approach addresses both goals, our primary emphasis is upon achieving computation tractability through data reduction.

Several choices present themselves when performing whole brain parcellation of resting state data. The similarity metric employed can affect the interpretation as well as the validity of the resulting clusters. A method for clustering across subjects must be chosen that generalizes well to single-subject data. Finally, the optimal number of clusters generated must be selected. Too few clusters will result in regions that are heterogeneous and information will be lost. Too many clusters will not result in information loss, but may not reduce the data to a computationally tractable size. We utilize a leave-one-out-cross-validation measure of reproducibility to evaluate different possibilities for each of these parameters.

4.1 Methods

4.1.1 Subjects and Scanning

Twenty four healthy control subjects (mean age 29, +/- 6.83, 9 females) were recruited in accordance with Emory University Institutional Review Board policy. To qualify for inclusion, subjects were required to be between the ages of 18 to 65, have no contraindications for MRI, to be medication free, and have no current or past neurological or psychiatric conditions.

Subjects were scanned on a 3.0T Siemens Magnetom TIM Trio scanner (Siemens Medical Solutions USA; Malvern PA, USA) using a 12 channel head matrix coil. Anatomic images were acquired at 1x1x1 mm3 resolution with an MPRAGE sequence using: FOV 224x256x176 mm3, TR 2600 ms, TE 3.02 ms, FA 8°, GRAPPA factor 2. Resting state fMRI data were acquired with the Z-SAGA sequence to minimize susceptibility artifacts [71]. One hundred and fifty functional volumes were acquired in thirty 4-mm axial slices using the parameters: TR 2920 msec, TE1/TE2 30 msec/66 msec, FA 90°, 64 x 64 matrix, in-plane resolution 3.44x3.44 mm^2.

For resting state functional scans, subjects were instructed to passively view a fixation cross while "clearing their minds of any specific thoughts." The fixation cross was used to discourage eye movement and help prevent subjects from falling asleep. Compliance was assessed during an exit interview; all subjects confirmed they had performed the task as requested without falling asleep.

4.1.2 Preprocessing

All preprocessing of MRI data was performed using SPM5 [39] running in MATLAB 2008a (The Mathworks; Natick MA, USA). Anatomic and fMRI data were evaluated for imaging artifacts such as excessive ghosting, banding, and other imaging errors; no images were removed. Anatomic scans were simultaneously segmented into white matter (WM), gray matter (GM), and cerebral-spinal fluid (CSF) and normalized to the ICBM462 normalized brain atlas. fMRI volumes were slice timing corrected, motion corrected, written into ICBM462 space at 4x4x4 mm3 resolution using the transformation calculated on the corresponding anatomic images, and spatially smoothed using a 6-mm FWHM Gaussian kernel. No images were removed due to excessive head motion (max motion < 1.75 mm, mean .87 mm +/- .43). fMRI data were restricted to gray matter and de-noised by regressing out motion parameters, WM time-course, as well as CSF time-course [89, 72]. Each voxel time-course was band-pass filtered (0.009 Hz < f < 0.08 Hz) to remove frequencies not implicated in resting state functional connectivity [33, 89] and then z-score normalized.

4.1.3 Whole Brain Clustering of Resting State Data

4.1.3.1 Normalized Cut (Ncut) Spectral Clustering

Normalized cut spectral clustering (Ncut) begins by representing resting state data as an undirected weighted similarity graph, $G = (V, E)$, with N vertices, V, corresponding to voxels and edges, E, connecting neighboring voxels [90]. Edges between two voxels, v_i and v_j, are weighted by the non-negative similarity, w_{ij}, of the voxels' FC. The algorithm proceeds by cutting the graph into a pre-specified number of clusters, K, such that the similarity between voxels within a cluster is greater than the similarity between voxels in

separate clusters. Several criteria have been proposed for determining optimal clustering. The minimum cut criterion solely minimizes the similarity between voxels in separate clusters, which will likely result in clusters which contain a single voxel. Normalized cut, on the other hand, normalizes the cut cost by the sum of edge weights within the cluster [91]. This results in partitions which are "balanced" as determined by the sum of edge weights within each cluster. Practically, G is represented as a NxN weighted adjacency matrix W (described in detail below) consisting of the edge weights, w_{ij}, and the Ncut problem is solved by linear algebra. Ncut clustering was performed using a Python implementation of the algorithm presented in [92].

4.1.3.2 Subject specific similarity matrices

Each w_{ij} of W corresponds to the similarity between the functional connectivity of two voxels, v_i and v_j, which are separated by a distance d_{ij}:

$$w_{ij} = \begin{cases} s(v_i, v_j) & d_{ij} \leq \varepsilon \\ 0 & d_{ij} > \varepsilon \end{cases}. \tag{21}$$

The radius ε was chosen to include the twenty-six nearest neighbors (3D neighborhood) of a voxel. This constrained the resulting clusters to contain contiguous, rather than spatially distributed, voxels. An additional benefit of the nearest-neighbor constraint is that it results in sparse similarity matrices which reduce computational overhead.

The similarity of functional connectivity between voxels, $s(v_i, v_j)$, can be defined in a number of ways. A common approach is to use the similarity between time-courses extracted from the voxels [83]. Another is to use extracted time-courses to first generate a whole brain FC map for each voxel and then measure the spatial similarity between these FC maps [88]. A metric for measuring similarity must also be chosen. An obvious choice is Pearson's correlation coefficient, which is only appropriate if a threshold is applied to make it non-negative. This approach ignores information that is present in negative correlations. An alternative is the eta^2 statistic [88] which is very similar to Pearson correlation for

normalized (mean centered, standard deviation =1) values and is non-negative:

$$eta^2 = \frac{SS_{withen}}{SS_{total}} = 1 - \frac{SS_{between}}{SS_{total}} = 1 - \frac{\sum_n[(v_i(n) - m(n))^2 + (v_j(n) - m(n))^2]}{\sum_n[(v_i(n) - \bar{M})^2 + (v_j(n) - \bar{M})^2]}. \quad (22)$$

Here n corresponds to a sample of a time series or a voxel of a FC map, $m(n)$ is the mean of $v_i(n)$ and $v_j(n)$, and $\bar{M}$ is the grand mean value of m. Applying eta^2 to voxel time series will be referred to as $t - eta^2$ and eta^2 between FC maps will be referred to as $s - eta^2$.

The choice between using $t - eta^2$ and $s - eta^2$ is application specific. $t - eta^2$ is desired when temporal homogeneity within a cluster is desired, whereas $s - eta^2$ is used when homogeneity of FC maps is preferred. At first consideration, these should be quite similar, since they are both determined by the voxel time-courses, but Figure 9 illustrates that while the two are highly correlated, their relationship is non-linear. Both $t - eta^2$ and $s - eta^2$ were employed to compare their relative merits.

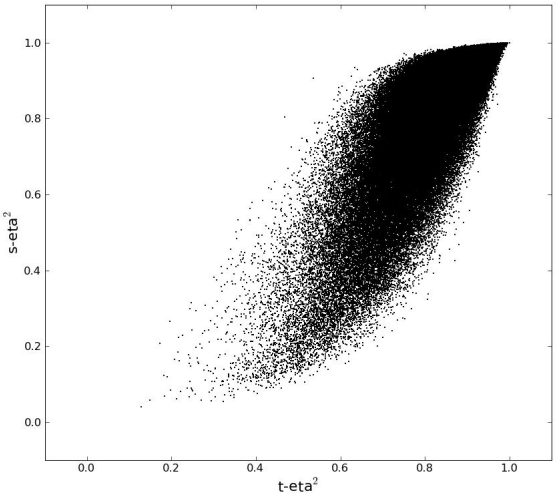

Figure 9. Comparison of $s - eta^2$ and $t - eta^2$ similarity metrics calculated from the resting state data of a single subject.

4.1.3.3 Clustering

Clustering was performed after individual specific similarity matrices were constructed. Clustering the group data was accomplished either by averaging the individual similarity

matrices and then submitting the average to clustering [87] or by performing clustering for each individual followed by a second level group clustering [83]. In the second case, an NxN adjacency matrix A was constructed for each subject from the results of the first level clustering. The elements a_{ij} of A equal one if both v_i and v_j were contained in the same cluster and zero otherwise [83]. The adjacency matrices were averaged across subjects to form a group coincidence matrix which is subsequently clustered using the Ncut algorithm. The first method resulted in faster computation since clustering must only be performed once, but may result in poor quality clustering. Both of these methods were compared.

4.1.3.4 Model Selection

Clustering resting state data requires specifying a similarity metric ($t - eta^2$ or $s - eta^2$), choosing group mean clustering or two-level clustering, and determining the optimal number of clusters K. A performance metric is required to optimize these parameters. This was accomplished using a leave-one-out cross-validation (LOOCV) estimate of cluster reproducibility, which was inspired by the desire to generate a clustering that best represents the functional segregation inherent at the individual level. LOOCV is an iterative procedure in which group clustering is performed after excluding a single subject. The adjacency matrix generated from the group clustering with the i^{th} subject excluded, A_{-i} is compared to the adjacency matrix calculated by clustering the data from the i^{th} subject, A_i. Accuracy was calculated as the ratio of voxel connections present in both A_{-i} and A_i, to the number connections present in A_i. This value was averaged across all possible ways to exclude one subject:

$$acc = \sum_{i=1}^{N} \frac{|A_{-i} \cap A_i|}{|A_{-i}|}. \tag{23}$$

ROI atlases were constructed using each combination of analysis ($t - eta^2$,$s - eta^2$) and averaging (global mean, two-level clustering) for K between 50 and 1000 in increments of 50. The performances of the different parameters were compared using LOOCV

reproducibility. Once the best similarity metric and global clustering strategy was determined, the optimal number of clusters was investigated further by iterating this process using smaller increments of K.

4.1.3.5 ROI-ROI and ROI-voxel seed based FC analyses

The best ROI atlas, as determined by the LOOCV procedure, was used in two types of functional connectivity analysis. These were performed to illustrate that the ROI atlas can produce networks consistent with those commonly reported in the literature. Seed ROIs from the atlas were chosen in the ventral posterior cingulate cortex (vPCC), left primary motor cortex (lM1), and left Brodmann area 17 (lBA17) to generate FC maps of the default mode network, motor network, and visual network respectively. Two methods were employed. In the first method, for each subject, time-courses were extracted for each ROI in the atlas, and summarized as the first eigenvector of a singular value decomposition [74]. The time-courses of the three seed ROIs were correlated with the time-courses of every other ROI in the atlas. The resulting Pearson's correlation coefficients were transformed to z-scores using Fisher's transform. FC maps for each seed ROI were summarized across subjects using one-sample t-tests. The results of the t-tests were FDR corrected, converted to a z-score, written back to every voxel in their respective regions in the ROI atlas, and displayed at an FDR corrected $p < 0.005$. In a second functional connectivity analysis, a similar procedure was followed, except that the time-course of each seed ROI was correlated with every other voxel in the brain.

4.2 Results

Whole brain parcellation of resting state data was performed using every combination of similarity metric, and group level clustering method ($s-eta^2$ group mean, $s-eta^2$ two-level, $t-eta^2$ group mean, and $t-eta^2$ two-level) for K between 50 and 1000, in multiples of 50. The resulting cluster maps were submitted to the LOOCV procedure for comparison; these results are shown in Figure 10. The two-level approach dramatically outperforms the group

mean. The $t - eta^2$ similarity metric combined with two-level group clustering is the clear winner. Optimal clustering appears to be contained within the plateau ending at $K = 300$; this reliability plateau is investigated further below.

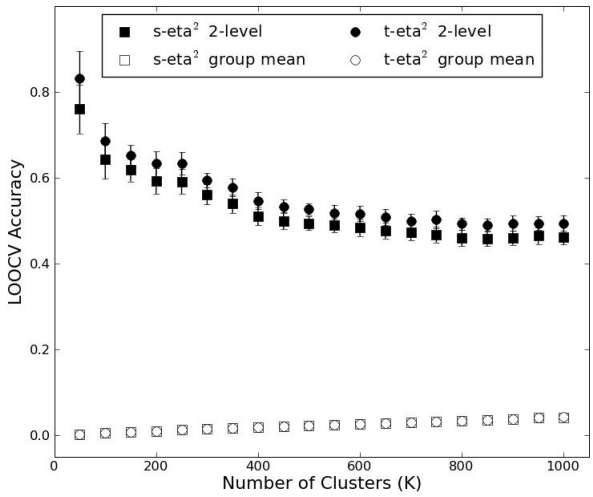

Figure 10. Comparison of LOOCV accuracy for each combination of parcellation strategy ($s - eta^2$ group mean, $s - eta^2$ two-level, $t - eta^2$ group mean, and $t - eta^2$ two-level) for K between 50 and 1000, in multiples of 50.

Figure 11 depicts parcellation results for $s - eta^2$ and $t - eta^2$ for choice of 50, 200, and 1000 ROIs. Note that ROI numbering (and thus, color coding) by the parcellation method is arbitrary; the 50 and 200 ROI maps have been re-colored to emphasize the ROI homology across analysis methods. (While the 1000 ROI parcellation also appears to bear homology across methods, re-coloring was too subjective due to the small size and large number of ROIs.) Both parcellation methods produced ROIs of similar shape, size, and location with variations around ROI borders.

Figure 11 also demonstrates that the number of ROIs being estimated strongly influences the interpretation of resulting ROI maps. Choosing too few ROIs (as in the 50 ROI parcellation) produced broad, over-generalized ROIs. This parcellation has numerous examples of functionally and anatomically distinct regions (e.g., hippocampus and amygdala; basal ganglia and thalamus; superior parietal lobule and supramarginal gyrus) being

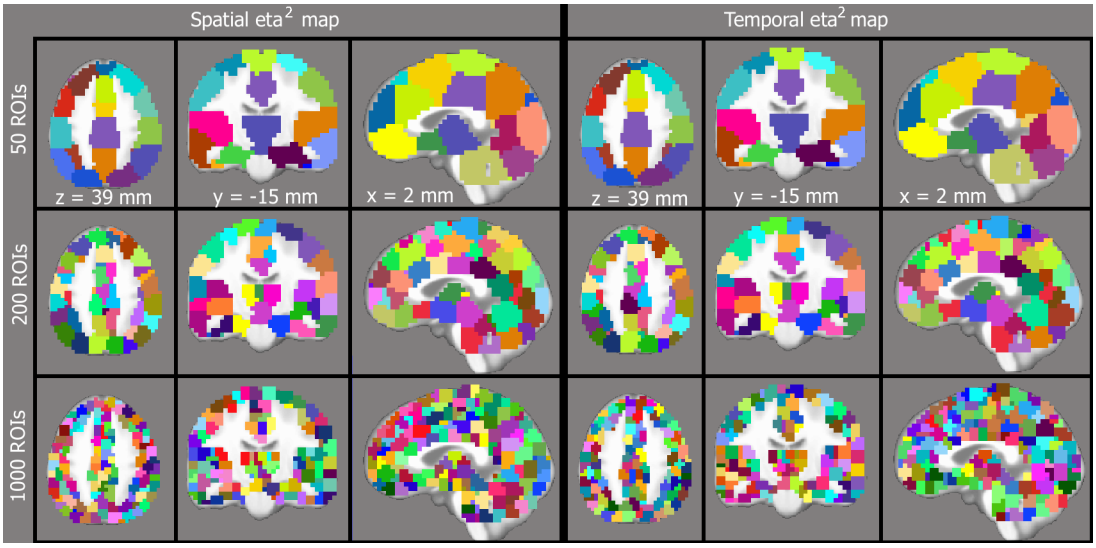

Figure 11. Comparison of parcellations by method ($s - eta^2$ or $t - eta^2$) and number of ROIs generated (50, 200, or 1000).

condensed into a single ROI. Conversely, too many ROIs (as in the 1000 ROI parcellation) produced scattered ROI maps of questionable interpretation value. For example, this parcellation divides the anterior cingulate into approximately 40 ROIs, whereas previous parcellations of the cingulate suggest fewer than 10 anatomically, functionally and histologically distinct subunits [80, 79, 93].

Qualitatively, the 200 ROI parcellation is a good compromise between these two extremes. ROIs are suitably large to accommodate individual anatomic variability. For example, the location of the primary motor cortex hand knob averages 31 mm from the midline, with a width of approximately 14 mm [94]. The distal range of the 200 ROI map's primary motor cortex ROI is 24mm – more than sufficient to house the hand knob. Yet the 200 ROI parcellation map is suitably small to discriminate primary motor from premotor – which is not possible for the 50 ROI map.

The two-level $t - eta^2$ group parcellation was next performed for cluster numbers between 50 and 300 in increments of 10 to establish an optimal number of clusters. The results of this analysis are shown in Figure 12. At the low end ($K < 90$), LOOCV reproducibility is high due to the large size of the ROIs. Further inspection proves that ROI maps generated

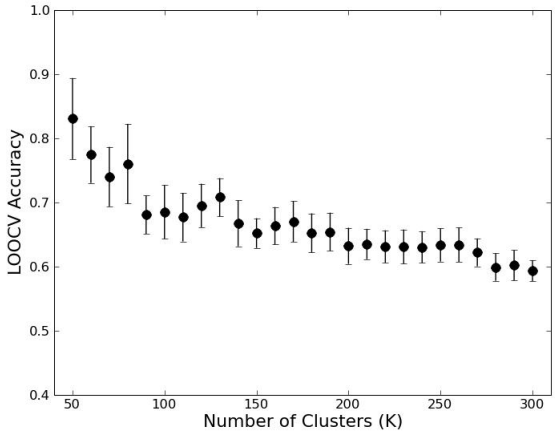

Figure 12. Comparison of LOOCV accuracy for each $t - eta^2$ two-level for K between 50 and 300, in multiples of 10.

at this level are obviously under-clustered and do not respect neuroanatomical boundaries. There is a subsequent peak at 130 clusters that we interpret as optimal. The 130 ROI map is illustrated in Figure 13.

There is substantial overlap between ROI-ROI and ROI-voxel functional connectivity maps generated for the vPCC, lM1, and lBA17 (Figure 14). The vPCC seed showed positive correlation with regions involved in the default mode network, including medial prefrontal cortex and bilateral superior parietal cortex, insula, and hippocampus. The parcellated vPCC region also showed negative correlation with midanterior cingulate. The lM1 seed elicited positive correlation with components of the resting-state motor network, including SMA, lateral prefrontal cortex, supramarginal gyrus, and superior cerebellum. Finally, the lBA17 seed produced positive correlation with the visual system, extending along both the ventral visual stream (into fusiform and parahippocampal gyrus) and the dorsal visual stream (into parietal cortex).

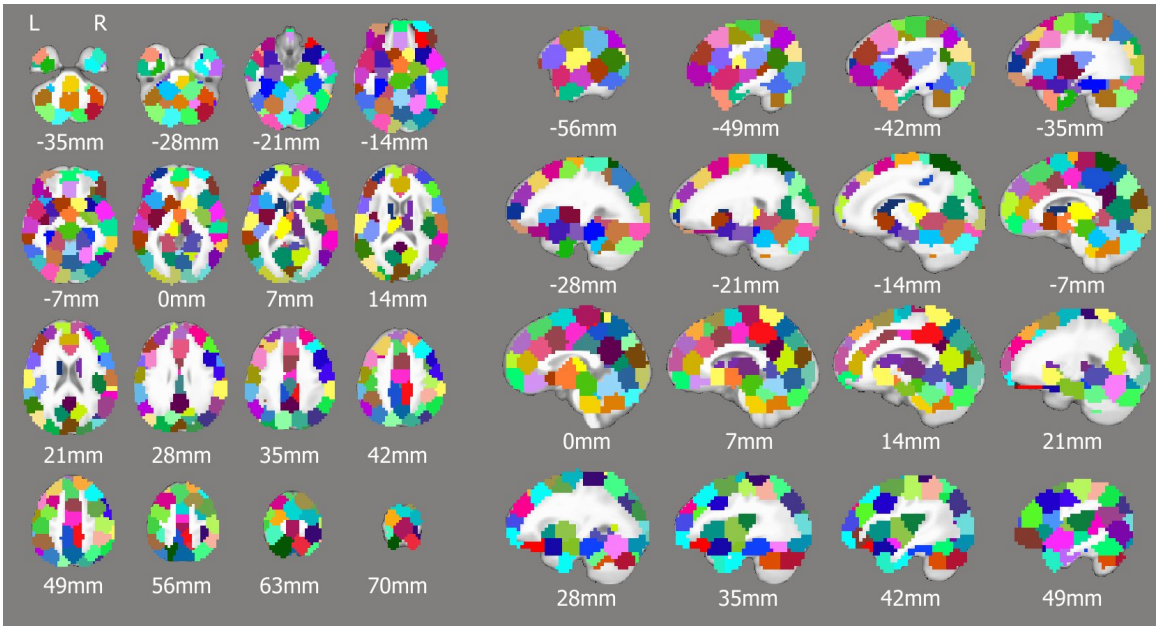

Figure 13. The $t-eta^2$ 130-ROI parcellation, shown in axial and sagittal slices (neurological convention).

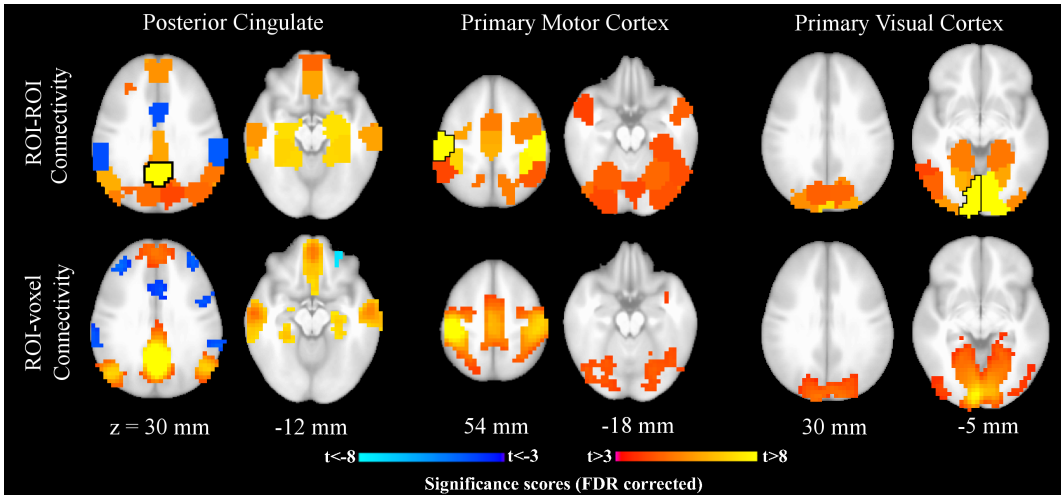

Figure 14. Comparison of parcellation-based and voxel-wise functional connectivity maps.

4.3 Discussion

The goal of the present resting-state clustering algorithm is to generate an ROI atlas that will be applicable to whole brain studies of functional connectivity. As such, it is important that group-level clustering fits individual subject data well, as future applications will depend on generalization to new datasets. In order to evaluate this, we used a leave-one-out cross-validation approach to measure how well an ROI atlas generated for a sample generalizes to individual subjects. This criterion was used to compare several methodological choices for performing group-level clustering (Figure 10). From this comparison, it is evident that the group mean approach did not generalize well to single subject data. The likely source of this poor performance was that the averaging process smooths functional boundaries between regions. On the other hand, in the two-level approach, subject-specific data was first clustered, and the results of this clustering were then averaged. We believe that this second approach better preserved the functional boundaries present in the data and thus has better generalization across subjects.

The difference between $t - eta^2$ and $s - eta^2$ similarity metrics is small, but significant. In Figure 11, overall clustering generated by the two different metrics is very similar. We believe small differences at ROI boundaries are responsible for the differences in LOOCV accuracy between the two approaches (Figure 10). Based on the LOOCV procedure, we concluded that the combination of $t - eta^2$ with the two-level clustering procedure is best.

Our approach depends upon a priori selection of how many ROIs to generate. Consequently, this selection is a concerning source of error. Selecting too few ROIs would be expected to produce parcellations of overly broad ROIs that lack ecological validity. For example, the parcellation of 50 ROIs in Figure 11 has one ROI encompassing both hippocampus and amygdala, despite their known functional independence. Other regions that are erroneously collapsed into a single ROI include basal ganglia and thalamus, orbitofrontal and medial prefrontal cortices, brainstem and cerebellum, and superior parietal lobe and supramarginal gyrus. The over-selection of ROIs is likewise problematic. The

goal of parcellation is to reduce the data dimensionality into functional subcomponents. Ideally, these subcomponents will be readily interpretable and reduce the computational complexity of future analytic methods. But as evidenced by the extreme example of 1000 ROIs, the resulting parcellation remains difficult to interpret. While this parcellation respects some neuroanatomic boundaries (such as separating amygdala and hippocampus), other divisions (such as splitting amygdala into four quadrants) lack literature support. Choosing the optimal number of ROIs to generate remains a critical methodological constraint.

We addressed this limitation by using leave-one-out cross-validation to optimize ROI selection (Figure 12). Our goal in using cross-validation was to identify the maximum number of ROIs that remained highly replicable for our sample. Parcellation was performed for K between 50 and 300 in steps of 10; this range was chosen from parcellations performed for a larger range of K (Figure 10). Parcellations generating 90 or less ROIs show high mean LOOCV accuracy, but also have high variance, indicating that some subjects did not fit these group level clusters well. These also fall into a "trivial" range, where ROIs are so large that high reproducibility is almost a certainty. We identified a peak in reproducibility for 130 ROIs; choosing this number of ROIs produces a parcellation which, upon visual inspection, respects most established neuroanatomic segregations.

Our 130 ROI parcellated brain has several features that indicate strong ecological validity. Chief among these is the bilateral symmetry of the two hemispheres. Most left-hemisphere ROIs share commensurate size, shape and location with their right-hemisphere counterparts. Bilateral symmetry has been reported for many of the cortical regions demonstrating symmetry in our parcellation, including the sensorimotor cortex (BA4,3,1,2), lateral premotor cortex (BA6), visual cortex (BA17) (extending into both dorsal and ventral streams), caudate, thalamus, hippocampus, and cerebellum. Similarly, parcellated regions lying along the midline, such as the anterior cingulate and supplementary motor area (SMA), are bilateral. Although these regions have distinct hemispheric segregation at the

neuronal level, their BOLD activities often manifest bilaterally [95, 96, 97, 98].

The segregation of the cingulate gyrus also reflects neuroanatomical boundaries defined by cyto-architectonics. First, the cingulate is separated from more dorsal regions, such as frontal eye fields (BA8), supplementary motor area (BA6), sensorimotor cortex, and superior parietal lobule (BA7). Parcellations with fewer ROIs (i.e. the 50 ROI parcellation) did not accurately reflect these well established neuroanatomic cortical boundaries. Second, the parcellation of the cingulate into fewer than ten sub-regions is supported by anatomic [79], functional [80], and multi-receptor autoradiography [93], suggesting high ecological validity for this approach.

As an additional means to assess ecological validity and to illustrate two ways in which the ROI atlas can be applied to functional connectivity analysis, parcellated regions' time-courses were used to derive functional connectivity maps (Figure 14). The correlation maps derived from ROI-ROI correlations are remarkably consistent with the ROI-voxel analysis. All voxels within the seed ROI show strong correlation with that ROI's time-course, indicating that the Ncut method is grouping voxels into meaningful clusters.

Additionally, the parcellation connectivity maps reflect correlations that have been reliably replicated in the literature. For example, the bilateral resting-state connectivity of the primary motor cortex with SMA, lateral premotor, supramarginal gyrus, and cerebellum has been well established [31, 47]. The consistency of these parcellated connectivity maps further confirms the validity of this clustering approach.

The ROI-ROI connectivity maps include some regions not included in the ROI-voxel counterparts. Upon further inspection, these regions are correlated but are slightly sub-threshold in the ROI-voxel maps. This can be attributed to the gain in SNR generated by summarizing time-courses within the ROIs, and also the massive reduction in multiple comparisons in the ROI-ROI compared to ROI-voxel analysis. It also should be noted that the ROI-voxel connectivity maps frequently produce clusters of smaller volume than the parcellated ROIs. For example, the hippocampal voxels that are correlated with posterior

cingulate are but a subset of the parcellated hippocampus ROI. However, this caveat is true for all ROI atlases. Voxel-wise analyses will always carry specific information that is missing from more generalized ROI atlases. Likewise, ROI atlases are valuable for dimensionality reduction – in this case, improving the efficacy of computationally intensive analyses.

4.4 Conclusion

In summary, we have introduced a data-driven method for parcellating the brain into functional subcomponents by resting-state connectivity. We have also introduced a metric for comparing the various trade-offs inherent in this task and applied this metric to determine the best measure of similarity, optimal strategy to perform parcellation across subjects, and the best number of parcellated regions. The result is an atlas of 130 functionally homogeneous ROIs that are suitable for investigating whole brain functional connectivity. This ROI atlas will be made available for use by the scientific community.

CHAPTER 5

WHOLE BRAIN FUNCTIONAL CONNECTIVITY ANALYSIS OF MAJOR DEPRESSIVE DISORDER

The previous chapters have focused on developing methods for applying support vector classification to predict disease states from functional connectivity. Specifically, they have focused on clustering whole-brain resting state fMRI data to reduce the number of brain regions to a computationally tractable size and the further reduction of features generated from these brain regions to those most useful to the disease state prediction problem. In this chapter we combine these contributions to perform a whole brain functional connectivity analysis of major depressive disorder (MDD). After the most relevant features for classification are derived, different methods for visualizing these features are explored. The objective of this chapter is to identify a pattern of functional connectivity (biomarker) that is capable of distinguishing patients in a current episode of MDD from healthy controls.

State-of-the-art functional connectivity group-level analyses evaluate the impact of disease on a set of hypothesized regions or networks (citations). While these studies have been successful at identifying functional connectivity differences in disease, they are limited by the hypotheses that specified the brain regions or networks. Indeed, many of the regions or networks employed in these analyses have been identified by task-based functional studies or hypotheses based on disease symptoms and brain regions (networks) implicated in the underlying processes involved in those symptoms. In contrast whole-brain functional connectivity analysis implies a hypothesis generating approach in which all possible functional connectivities between brain regions are tested to see if they differ between disease states. In the predictive modeling setting, this approach has the possible benefit of improving prediction accuracy by incorporating regions not previously implicated in the disease process.

There is a growing concensus on the brain regions implicated in MDD, yet not all of

these regions are reported in all studies, and there is variability in whether these regions are found to be up-regulated or down-regulated in depression. These discrepancies suggest that the connectivity between regions is more relevant to the disease state than localized differences [73]. Indeed, structural equation modeling performed on resting state PET FDG data has found effective connectivity differences (directional functional connectivity) capable of differentiating response to treatments of depression [99]. A few studies have investigated resting state fMRI functional connectivity in depression. Altered connectivity between the default mode network, a network known to involve several brain regions implicated in depression, and the subgenual cingulate cortex and thalamus have been identified in an independent components analysis [18]. Additionally functional connectivity differences have been found between the pregenual anterior cingulate and members of the limbic system (amygdala, pallidostriatum, medial thalamus) in unipolar depression [100] and further investigation found that these differences were more exaggerated in bipolar depressed subjects [101]. These differences in functional connectivity between the anterior cingulate and limbic regions are impacted by anti-depressant medications [102, 101]. While these studies have found targeted differences in functional connectivity, they do not characterize all of the functional connectivity differences present in depression, nor do they investigate the utility of these regions as a biomarker for the disease. These goals can be accomplished by applying SVC analysis to whole brain functional connectivity.

A major obstacle to applying SVC analysis to biomarker discovery is extracting the brain regions important to the classification as well as determining how these regions differ between disease states. While extracting brain regions from the classifier can be accomplished using feature selection, it is difficult to rank the regions in terms of their importance. Additionally identifying how the functional connectivities differ between disease states is of interest. A standard approach available to linear SVC is to rank the most relevant features by a feature score calculated from the discriminating hyperplane, and to assume that the sign of this rank is indicative of how a feature differs between groups. We explore this

method and propose an additional visualization method that identifies hubs in the functional connectivity network.

5.1 Methods

5.1.1 Subjects

Seventy-nine subjects were recruited in accordance with Emory University Institutional Review Board policy. Forty-five subjects (MDD; 17 female, mean age 42.6 +/- 11.3) met DSM IV criteria for a current major depressive episode without any co-morbid psychiatric disorders and had a minimum 17-item Hamilton Depression Rating Scale (HDRS) score of 15 (mean 18.7 +/- 3.2) at the time of scanning. Thirty-four healthy controls (HC; 16 female, mean age 30.7 +/- 7.8) with no history of major depression or current diagnosis as determined by DSM IV criteria were recruited for comparison. To qualify for inclusion subjects were required to be between the ages of 18 to 65, have no contraindications for MRI procedures, to be medication free, and without history of current or past neurological or psychiatric conditions.

There is a significant difference in age ($p = 1.33 \times 10^{-6}$) and motion ($p = 0.012$) between MDD and HC subjects. To account for these differences subjects were further subdivided into training (MDD-T, HC-T) and holdout validation (MDD-HO, HC-HO) groups which are described in Table 5. The training groups will be used to develop a classifier, and its performance will be evaluated on the holdout groups.

Table 5. Subject groups

Group	# Subjects	# Females	Age (years)	Motion (mm)	HDRS
HC-T	25	11	33.4 +/- 7.3	.8 +/- .4	N/A
MDD-T	25	11	34.7 +/- 8.1	.7 +/- 3	18.4 +/- 2.7
HC-HO	9	5	**23.1 +/- 1.9**	**.9 +/- .4**	N/A
MDD-HO	20	6	**52.4 +/- 5.4**	**.5 +/- .2**	19.2 +/- 3.8

5.1.2 Scanning

Subjects were scanned on a 3.0T Siemens Magnetom TIM Trio scanner (Siemens Medical Solutions USA; Malvern PA, USA) using a 12- channel head-matrix. Anatomic images were acquired at $1 \times 1 \times 1 mm^3$ resolution with an MPRAGE sequence using: FOV $224 \times 256 \times 176 mm^3$, TR 2600 msec, TE 3.02 msec, FA 8°, GRAPPA factor 2. Resting state fMRI data were acquired with the Z-SAGA sequence to minimize susceptibility artifacts [71]. One hundred and fifty functional volumes were acquired in thirty 4-mm axial slices using the parameters: TR 2920 msec, TE^1/TE^2 30 msec/66 msec, FA 90°, 64×64 matrix, in-plane resolution $3.44 \times 3.44 mm^2$.

For resting state functional scans, subjects were instructed to passively view a fixation cross while "clearing their minds of any specific thoughts." The fixation cross was used to discourage eye movement and help prevent subjects from falling asleep. Compliance was assessed during an exit interview; all subjects confirmed they had performed the task as requested without falling asleep.

5.1.3 Preprocessing

All preprocessing of MRI data was performed using SPM5 [39] running in MATLAB 2008a (The Mathworks; Natick MA, USA). Anatomic and fMRI data were evaluated for imaging artifacts such as excessive ghosting, banding, and other imaging errors; no images were removed. Anatomic scans were simultaneously segmented into white matter (WM), gray matter (GM), and cerebral-spinal fluid (CSF) and normalized to the ICBM462 normalized brain atlas. fMRI volumes were slice timing corrected, motion corrected, written into ICBM462 space at $4 \times 4 \times 4 mm^3$ resolution using the transformation calculated on the corresponding anatomic images, and spatially smoothed using a 6-mm FWHM Gaussian kernel. No images were removed due to excessive head motion (max motion < 1.75 mm). fMRI data were restricted to gray matter and de-noised by regressing out motion parameters, WM time-course, as well as CSF time-course [89, 72]. Each voxel time-course was band-pass filtered ($0.009 Hz < f < 0.08 Hz$) to remove frequencies not implicated in resting

state functional connectivity [33, 89].

5.1.4 ROI Time Course Extraction

Region of interest (ROI) time-course extraction was performed using the AFNI tool-set (Cox 1996; Cox and Hyde 1997). ROIs were defined by a 130-region atlas that was derived by parcellating the whole brain functional connectivity data of 24 healthy control subjects (Chapter 4). For each subject, ROIs were restricted to gray matter using the subject's gray matter mask. Time-courses were extracted from every voxel in a ROI and reduced to the first eigenvariate from singular value decomposition [74]. This procedure was performed for every region in the ROI mask, resulting in 130 time-courses per subject.

5.1.5 SVC of Functional Connectivity

SVC of functional connectivity was performed using custom scripts running in MATLAB using the SVC functions from the Bioinformatics Toolbox. All unique pairwise correlations of ROI time-courses were calculated for each subject resulting in 8385, $(\frac{1}{2}\times130\times(130-1))$, correlation coefficients per subject. Correlation coefficients were converted to z-scores using the Fisher transform. The resulting correlation maps for MDD-T and HC-T groups were entered into a linear support vector classification (SVC) analysis to discriminate MDD from HC. The box constant was set to 1,000,000 (hard margin) following previous observations that this is sufficient for fMRI data [21, 23].

Reliability filter (RF) feature selection was performed to reduce the input space to those features most relevant to the classification problem (Chapter 3). Distributions were estimated for each feature's corresponding SVC weight using 10,000 iterations of bootstrap resamplings. Using the assumption that the SVC weights are normally distributed, a reliability score for each feature is calculated from:

$$FS_i = \frac{\bar{x}_i}{\sigma_i}, \tag{24}$$

where $\bar{x}_i$ and σ_i are the mean and standard deviation of the SVC weights corresponding to

the i^{th}feature. A threshold was applied to the features scores to reduce the feature set to just the most reliable features.

The optimal threshold for feature selection was chosen using a model selection procedure. The range of feature scores between 1.96 (corresponding to 95% confidence intervals) and the maximum feature score obtained was split into ten intervals. The threshold corresponding to each interval was used to exclude features and the remaining features were submitted to a leave-one-out cross-validation (LOOCV) procedure to obtain threshold specific estimates of prediction error. After the ten thresholds have been evaluated, the threshold with the lowest prediction error, and fewest retained features was chosen as the optimal threshold.

After feature selection was performed, a classifier was obtained by training SVC on the training data (MDD-T and HC-T) using only the features retained after feature selection. The trained classifier was then used to predict the disease state (MDD or HC) of the hold-out groups and these predictions were used to calculate prediction error for the classifier. The linear hyperplane corresponding to the classifier was then visualized to determine the functional connectivity patterns that discriminate subjects with depression from healthy controls.

A null hypothesis test was constructed for the hold-out cross-validation procedure by assuming that misclassifications are i.i.d. $Bernoulli(p)$, where p is the probability of a misclassification due to chance [103, 20]. The number of misclassifications will follow a $Binomial(n, p)$ distribution, where n is the number of test examples (size of hold-out group). The probability of a misclassification due to chance is:

$$p(\hat{y}_i \neq y_i) = p(\hat{y}_i = 1|y_i = -1) + p(\hat{y}_i = -1|y_i = 1) \tag{25}$$

$$p(\hat{y}_i \neq y_i) = p(\hat{y}_i = 1)p(y_i = -1) + p(\hat{y}_i = -1)p(y_i = 1), \tag{26}$$

where $\hat{y}_i$ is the predicted label for the i^{th} hold-out observation. Equation (26) follows from

the fact for chance the prediction is completely independent of the true label of the observation. For this experiment the probabilities where $p(\hat{y}_i = 1) = .5$ and $p(\hat{y}_i = -1)$ (from the frequencies of the training data) and $p(y_i = 1) = 9/29$ and $p(y_i = -1) = 20/29$ (from the frequencies of the hold-out data). The resulting probability of misclassification is $p(\hat{y}_i \neq y_i) = .5$. The probability of obtaining an observed prediction error using the trivial classifier (null hypothesis) was determined from this distribution [103, 20].

5.1.6 Interpretation of SVC results

The features identified by the feature selection algorithm were ranked by feature score (equation 24) to determine the features most relevant to disease. Additionally a feature-specific between group t-test was performed on the training data and compared to feature score to determine if the sign of the feature score is indicative of how the feature differs between disease states. A SVC classifier was trained using each feature alone and used to predict the hold-out group. The prediction accuracy obtained was compared with the feature score to determine how well the feature score indicates the prediction performance of the feature.

In order to visualize the importance of brain regions to the prediction task, each brain region was annotated by the maximum feature score obtained across all features in which that brain region participates. Additionally the number of features that each brain region is implicated in was calculated to identify hubs in the functional connectivity network. These two statistics were written back to the ROI mask and overlaid on a T1 to aid in localization of brain regions implicated by the features.

5.2 Results

The feature selection threshold is optimized during the model selection procedure. Ten thresholds are tested ranging between 1.96 and the maximum feature score obtained. For each threshold a LOOCV estimate of prediction error is obtained. This results are illustrated in Figure 15. The 1.96 minimum threshold guarantees that the 95% confidence

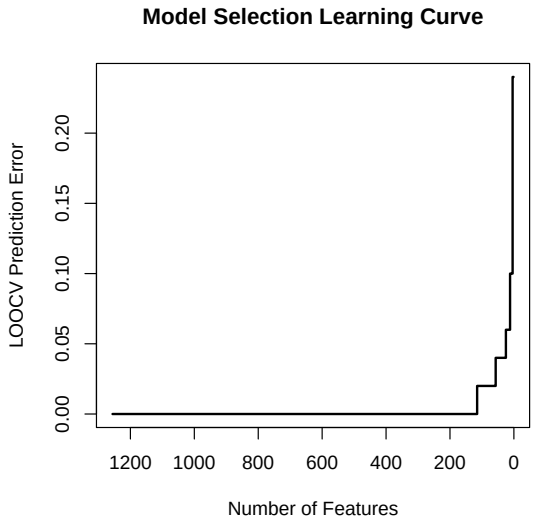

Figure 15. Learning Curve

intervals do not include zero, this minimum level of reliability results in zero prediction error. As the threshold increases, it eventually reaches a level were prediction error degrades. The minimum number of features that produces zero LOOCV prediction error is 115. A SVC classifier was trained on these features and all of the training data and used to classify the observations in the hold-out data sets. This classifier was able to correctly predict the disease status of 26 of the 29 hold-out subjects, for a prediction accuracy of 89.6% which is significantly better than what is obtainable by chance ($p = 6.8 \times 10^{-6}$). Of the three subjects that were mispredicted one was a healthy control and the remaining two suffer from depression.

The 115 features chosen by the RF procedure are listed in Table 6 along with their feature score, the hold-out prediction accuracy for the single feature, and the results of a between group t-test performed on the feature presented as the t-score and FDR corrected p-value. There is not a significant linear relationship between a feature's score and the hold-out cross-validation error calculated using only that feature as determined by Pearson's correlation ($\rho = -.15378,\ p = .1$). The feature that has the best prediction accuracy when taken alone is right posterior hippocampus <-> right cerebellum which is ranked 39^{th}

by feature score and is not significantly different as determined by the t-test. The t-test at a FDR corrected $p < .05$ finds 30 of the 115 features identified by SVC. Comparison of t-scores with feature scores indicates that the sign is identical between these two statistics (Figure 16). Thus indicating that a positive feature score indicates that functional connectivity in HC is greater than that in MDD and vice-versa.

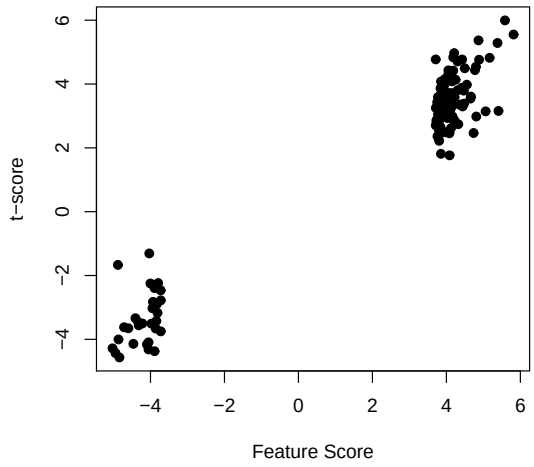

Figure 16. Comparison of t-scores to feature scores.

The 115 features represent the functional connectivity between 85 distinct brain regions. In order to visualize the importance of different brain regions to the SVC classifier, each brain region was assigned the maximum feature score from the features that contain that brain region. This is illustrated in Figure 17. This allows the localization of regions implicated in the highest ranking features, but does not represent the functional connectivities of these regions. The 11 regions implicated in the 8 highest ranking features are inferior brain stem, left cerebellum, left parahippocampal gyrus, left primary motor, left superior frontal gyrus (BA 9), mid-line cerebellum (IX), mid-line cerebellum (vermis/V), right caudate/putamen, right parahippocampal gyrus, right superior middle frontal gyrus (BA 10), and the rostral anterior cingulate (BA 24).

Any region that is involved in several features is a hub in the depression network. These

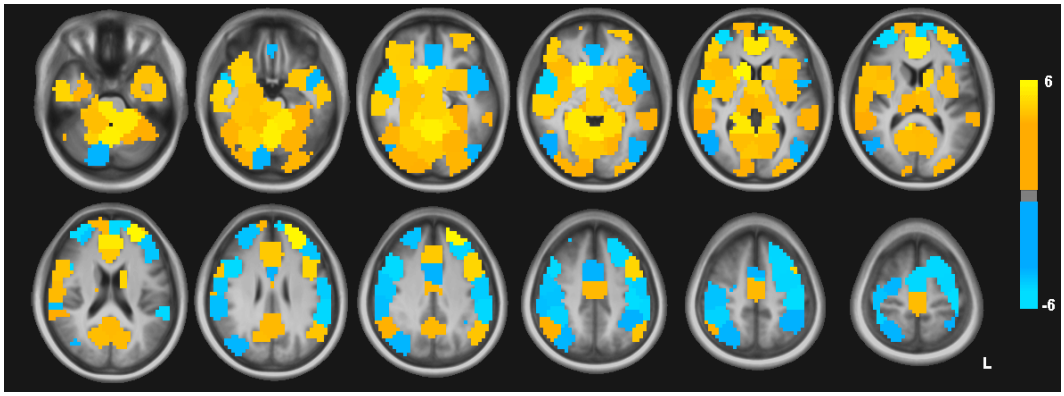

Figure 17. Maximum feature scores for brain regions implicated in classifier.

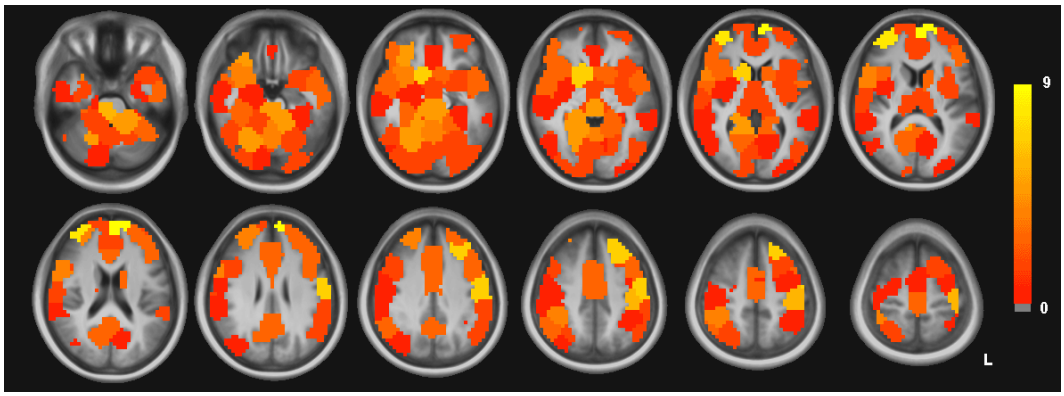

Figure 18. Number of features each brain region participates in.

hubs are likely foci of disease related dysfunction. In order to visualize these brain regions, the number of features that each brain region is involved in was calculated and is visualized in Figure 18. The top 5 regions have 7 or more connections and are left superior frontal gyrus (BA 10), right superior middle frontal gyrus (BA 10), right caudate/putamen, left frontal eye fields (BA 8) and left central sulcus.

5.3 Discussion

This study applies SVC to whole brain functional connectivity to determine patterns of functional connectivity capable of discriminating subjects with MDD from healthy controls. The resulting classifier achieved 89.6% prediction accuracy, which is significantly

Table 6. Top twenty features implicated by SVC

Region Name	Region Name	FS	HO CV	t	p (FDR)
left superior frontal gyrus (9)	right caudate/putamen	5.82	0.34	5.55	0.01
midline cerebellum (vermis/ V)	midline cerebellum (IX)	5.58	0.24	5.99	0
right parahippocampal gyrus	left cerebellum (III/ IV/ V)	5.41	0.31	3.16	0.11
inferior brainstem	rostral anterior cingulate (24)	5.38	0.45	5.29	0.01
inferior brainstem	midline cerebellum (vermis/ V)	5.17	0.31	4.82	0.02
left parahippocampal gyrus	left cerebellum (III/ IV/ V)	5.06	0.21	3.14	0.11
right superior middle frontal gyrus (10)	left primary motor (4)	-5.03	0.38	-4.28	0.03
right middle frontal gyrus (8)	left superior frontal gyrus	-4.95	0.48	-4.43	0.03
left parahippocampal gyrus	left primary motor (4)	4.88	0.31	4.76	0.02
left superior temporal gyrus (38)	left supramarginal gyrus (40)	-4.88	0.59	-1.67	0.4
left caudate	left middle frontal gyrus (8)	4.87	0.28	5.37	0.01
SMA (6)	left superior frontal gyrus (6)	-4.87	0.24	-4	0.06
left frontal eye fields (8)	left lateral premotor (6)	-4.84	0.34	-4.57	0.02
left superior temporal gyrus (38)	right inferior temporal gyrus	4.81	0.41	2.98	0.12
left caudate/putamen	rostral anterior cingulate (24)	4.8	0.41	4.54	0.02
hypothalamus	superior brainstem	4.77	0.24	4.44	0.03
right middle temporal gyrus (21)	right temporal pole	4.74	0.72	2.47	0.2
left frontal eye fields (8)	right inferior parietal lobe	-4.71	0.55	-3.62	0.1
right inferior frontal gyrus (45/47)	right fusiform / cerebellum (VI)	4.66	0.52	3.61	0.1

better than chance. The prediction accuracy reported here is a conservative estimate considering the substantial differences between the training and hold-out groups. The original data set had a significant difference in age and head motion between HC and MDD groups. Observations were assigned into training and hold-out groups such that the HC and MDD subjects in the training group are not significantly different in age or head motion and the remaining subjects were assigned to the hold-out groups. Thus, preventing age and head motion from confounding SVC training and providing a more rigorous hold-out validation.

Feature selection was performed using the reliability filter algorithm (Chapter 3). This algorithm initially removed the most unreliable features using a 95% confidence interval threshold. This first threshold reduced the featurespace to 1256 features which achieved a 0% LOOCV prediction error. This threshold was iteratively increased, and the threshold resulting in the fewest features without increasing LOOCV prediction error was selected as the optimal threshold (Figure 15). This threshold reduced the featurespace to 115 features (1.4% of the original 8385 features). The 1141 features that passed the less stringent threshold, but not the optimal threshold, are either unimportant to the classification task or highly correlated with the 115 features. If they are unimportant then retaining them would result in over-fitting and likely reduce the hold-out cross-validation prediction accuracy.

The 115 features selected by the RF algorithm involve 85 of the 130 brain regions in the ROI mask. A comparison of the hold-out cross-validation error obtained by just using each feature on their own to the reliability feature scores indicates that there is no linear relationship between the two (Table 6). It could be that the feature scores are not indicative of the predictive power of the features, or that the feature scores are sensitive to the importance of the multivariate relationships of the features. The observation that feature scores derived from SVC feature weights are not perfect indicators of a features impact on prediction performance has been made before [66]. The results of feature-specific t-tests did not correlate well with the univariate prediction performance of a feature either. In fact a between group t-test on the feature with the best hold-out cross-validation prediction

performance was not significant. Figure 16 illustrates that the sign of a feature-specific t-test comparing HC > MDD is positive so is the feature score and vice-versa. Thus a positive feature score indicates that the feature is on average higher in the HC group than the MDD group and that a negative feature score indicates that the feature is on average lower in the HC than MDD.

The top five features as measured by reliability feature score are the functional connectivities: left superior frontal gyrus (BA 9) <-> right caudate/putamen, mid-line cerebellum (vermis/V) <-> mid-line cerebellum (IX), right parahippocampal gyrus <-> left cerebellum, inferior brain stem <->rostral anterior cingulate, and inferior brain stem <->mid-line cerebellum (vermis/V).All of the brain regions associated with these features have been previously implicated in MDD [73, 104]. The previous finding that subgenual cingulate gyrus (BA 25) <-> default mode connectivity is different between MDD and HC [18] is not replicated in our results. The closest analog of the subgenual cingulate gyrus in our atlas, mid-line ventral orbitofrontal (BA 10) / subgenual cingulate (BA 32), showed altered connectivity with left caudate. The right caudate/putamen ROI appears to contain BA 25 and it has altered connectivity with left superior frontal gyrus (BA 9), right superior middle frontal gyrus (BA 10), left superior middle frontal gyrus (BA 10), left superior frontal gyrus, left middle frontal gyrus (BA 8), and left inferior middle frontal gyrus (BA 9) (Table 6). The frontal regions in BA10 and BA9 are a part of the default mode network, but other regions of this network such as hippocampus, posterior cingulate and bilateral parietal are not found to be different. Additionally altered connectivity of thalamus with the default mode network was not reproduced. Previous reports of decreased functional connectivity between rostral anterior cingulate and left caudate/putamen in MDD were reproduced, but not the other findings of rostral anterior cingulate with amygdala or thalamus [100, 102, 105, 101].

We propose two methods to visualize the brain regions involved in the features implicated in depression. In the first visualization brain regions are color coded according to the

feature score of the highest ranking feature that includes the brain region (Figure 17). The second color codes brain regions according to the total number of features that include the brain region (Figure 18). By comparing these two methods it is evident that left superior frontal gyrus (BA 10), right superior middle frontal gyrus (BA 10), right caudate/putamen, and mid-cingulate cortex (BA24) have a high feature score and have several connections. Most of these have been consistently implicated in neuroimaging literature on depression [73]. Other regions such as the rostral anterior cingulate (BA 24) have a high feature score, yet few connections. Indicating that while it may not be a hub, the functional connectivity of the rostral anterior cingulate (BA24) is important to the classifier. This region is strongly linked to depression [73, 100, 102, 105, 101]

5.4 Conclusion

This chapter reports on the first whole brain functional connectivity analysis performed in disease. We have developed a classifier that is capable of distinguishing patients with depression from healthy controls with a prediction accuracy of 89.6%. The classifier makes use of 115 bivariate correlations involving 85 distinct brain regions. Many of these regions have been previously implicated in depression by task based functional neuroimaging studies. We have also presented two visualization strategies to aid in the interpretation of the classifier.

CHAPTER 6

CONCLUSIONS

The work presented in this dissertation involves at least four novel contributions to functional connectivity analysis of resting state fMRI data. Support vector classification to functional connectivity analysis provides a means to identify multivariate patterns of functional connectivity capable of predicting disease state. The reliability filter feature selection algorithm provides a new means for identifying the features that are most relevant to the disease prediction problem that is grounded is statistical theory. Parcellating whole brain functional connectivity data reduces the input feature space makes whole brain functional connectivity analyses computationally feasible. And finally applying these techniques to predicting disease state from functional connectivity catalogues all of the functional connectivity differences important in depression. This work has resulted in one publication that is in press, one that is in submission, and a third publication that is still in preparation.

BIBLIOGRAPHY

[1] R. W. Thatcher, P. J. Krause, and M. Hrybyk, "Cortico-cortical associations and eeg coherence: a two-compartmental model," *Electroencephalogr Clin Neurophysiol*, vol. 64, pp. 123–43, Aug 1986.

[2] D. M. Tucker, D. L. Roth, and T. B. Bair, "Functional connections among cortical regions: topography of eeg coherence," *Electroencephalogr Clin Neurophysiol*, vol. 63, pp. 242–50, Mar 1986.

[3] B. Horwitz, "Functional interactions in the brain: use of correlations between regional metabolic rates," *J Cereb Blood Flow Metab*, vol. 11, pp. A114–20, Mar 1991.

[4] R. Matsumoto, D. R. Nair, E. LaPresto, I. Najm, W. Bingaman, H. Shibasaki, and H. O. Lüders, "Functional connectivity in the human language system: a cortico-cortical evoked potential study.," *Brain*, vol. 127, pp. 2316–2330, Oct 2004.

[5] R. Matsumoto, D. R. Nair, E. LaPresto, W. Bingaman, H. Shibasaki, and H. O. Lüders, "Functional connectivity in human cortical motor system: a cortico-cortical evoked potential study.," *Brain*, vol. 130, pp. 181–197, Jan 2007.

[6] S. J. Li, B. Biswal, Z. Li, R. Risinger, C. Rainey, J. K. Cho, B. J. Salmeron, and E. A. Stein, "Cocaine administration decreases functional connectivity in human primary visual and motor cortex as detected by functional mri," *Magn Reson Med*, vol. 43, pp. 45–51, Jan 2000.

[7] M. J. Lowe, M. D. Phillips, J. T. Lurito, D. Mattson, M. Dzemidzic, and V. P. Mathews, "Multiple sclerosis: low-frequency temporal blood oxygen level-dependent

fluctuations indicate reduced functional connectivity initial results," *Radiology*, vol. 224, pp. 184–92, Jul 2002.

[8] K. Wang, T. Jiang, M. Liang, L. Wang, L. Tian, X. Zhang, K. Li, and Z. Liu, "Discriminative analysis of early alzheimer's disease based on two intrinsically anti-correlated networks with resting-state fmri," *Med Image Comput Comput Assist Interv Int Conf Med Image Comput Comput Assist Interv*, vol. 9, no. Pt 2, pp. 340–7, 2006.

[9] L. Wang, Y. Zang, Y. He, M. Liang, X. Zhang, L. Tian, T. Wu, T. Jiang, and K. Li, "Changes in hippocampal connectivity in the early stages of alzheimer's disease: evidence from resting state fmri," *Neuroimage*, vol. 31, pp. 496–504, Jun 2006.

[10] M. D. Greicius, G. Srivastava, A. L. Reiss, and V. Menon, "Default-mode network activity distinguishes alzheimer's disease from healthy aging: evidence from functional mri," *Proc Natl Acad Sci U S A*, vol. 101, pp. 4637–42, Mar 30 2004.

[11] S. J. Li, Z. Li, G. Wu, M. J. Zhang, M. Franczak, and P. G. Antuono, "Alzheimer disease: evaluation of a functional mr imaging index as a marker," *Radiology*, vol. 225, pp. 253–9, Oct 2002.

[12] A. G. Garrity, G. D. Pearlson, K. McKiernan, D. Lloyd, K. A. Kiehl, and V. D. Calhoun, "Aberrant "default mode" functional connectivity in schizophrenia," *Am J Psychiatry*, vol. 164, pp. 450–7, Mar 2007.

[13] Y. Zhou, M. Liang, T. Jiang, L. Tian, Y. Liu, Z. Liu, H. Liu, and F. Kuang, "Functional dysconnectivity of the dorsolateral prefrontal cortex in first-episode schizophrenia using resting-state fmri," *Neurosci Lett*, Mar 12 2007.

[14] M. Liang, Y. Zhou, T. Jiang, Z. Liu, L. Tian, H. Liu, and Y. Hao, "Widespread functional disconnectivity in schizophrenia with resting-state functional magnetic resonance imaging," *Neuroreport*, vol. 17, pp. 209–13, Feb 6 2006.

[15] L. Tian, T. Jiang, Y. Wang, Y. Zang, Y. He, M. Liang, M. Sui, Q. Cao, S. Hu, M. Peng, and Y. Zhuo, "Altered resting-state functional connectivity patterns of anterior cingulate cortex in adolescents with attention deficit hyperactivity disorder," *Neurosci Lett*, vol. 400, pp. 39–43, May 29 2006.

[16] V. L. Cherkassky, R. K. Kana, T. A. Keller, and M. A. Just, "Functional connectivity in a baseline resting-state network in autism," *Neuroreport*, vol. 17, pp. 1687–90, Nov 6 2006.

[17] A. B. Waites, R. S. Briellmann, M. M. Saling, D. F. Abbott, and G. D. Jackson, "Functional connectivity networks are disrupted in left temporal lobe epilepsy," *Ann Neurol*, vol. 59, pp. 335–43, Feb 2006.

[18] M. D. Greicius, B. H. Flores, V. Menon, G. H. Glover, H. B. Solvason, H. Kenna, A. L. Reiss, and A. F. Schatzberg, "Resting-state functional connectivity in major depression: Abnormally increased contributions from subgenual cingulate cortex and thalamus," *Biol Psychiatry*, Jan 8 2007.

[19] D. D. Cox and R. L. Savoy, "Functional magnetic resonance imaging (fmri) "brain reading": detecting and classifying distributed patterns of fmri activity in human visual cortex.," *Neuroimage*, vol. 19, pp. 261–270, Jun 2003.

[20] T. M. Mitchell, R. Hutchinson, R. S. Niculescu, F. Pereira, X. Wang, M. Just, and S. Newman, "Learning to decode cognitive states from brain images," *Mach. Learn.*, vol. 57, no. 1-2, pp. 145–175, 2004.

[21] S. LaConte, S. Strother, V. Cherkassky, J. Anderson, and X. Hu, "Support vector machines for temporal classification of block design fmri data.," *Neuroimage*, vol. 26, pp. 317–329, Jun 2005.

[22] J. Mourão-Miranda, A. L. W. Bokde, C. Born, H. Hampel, and M. Stetter, "Classifying brain states and determining the discriminating activation patterns: Support

vector machine on functional mri data.," *Neuroimage*, vol. 28, pp. 980–995, Dec 2005.

[23] X. Chen, F. Pereira, W. Lee, S. Strother, and T. Mitchell, "Exploring predictive and reproducible modeling with the single-subject fiac dataset.," *Hum Brain Mapp*, vol. 27, pp. 452–461, May 2006.

[24] I. Guyon, J. Weston, S. Barnhill, and V. Vapnik, "Gene selection for cancer classification using support vector machines," *Mach. Learn.*, vol. 46, no. 1-3, pp. 389–422, 2002.

[25] S. M. LaConte, J. Chen, S. J. Peltier, and X. P. Hu, "Discriminating one finger from another: Support vector classification of event related fmri," in *Proceedings of the 13th Scientific Meeting of the International Society for Magnetic Resonance in Medicine, May 7-13, 2005, Miami, Florida*, 2005.

[26] J. Mourão-Miranda, E. Reynaud, F. McGlone, G. Calvert, and M. Brammer, "The impact of temporal compression and space selection on svm analysis of single-subject and multi-subject fmri data.," *Neuroimage*, vol. 33, pp. 1055–1065, Dec 2006.

[27] F. D. Martino, G. Valente, N. Staeren, J. Ashburner, R. Goebel, and E. Formisano, "Combining multivariate voxel selection and support vector machines for mapping and classification of fmri spatial patterns.," *Neuroimage*, Jul 2008.

[28] T. M. Mitchell, R. Hutchinson, M. A. Just, R. S. Niculescu, F. Pereira, and X. Wang, "Classifying instantaneous cognitive states from fmri data.," *AMIA Annu Symp Proc*, pp. 465–469, 2003.

[29] J. Mourão-Miranda, K. J. Friston, and M. Brammer, "Dynamic discrimination analysis: a spatial-temporal svm.," *Neuroimage*, vol. 36, pp. 88–99, May 2007.

[30] K. J. Friston, C. D. Frith, P. F. Liddle, and R. S. Frackowiak, "Functional connectivity: the principal-component analysis of large (pet) data sets," *J Cereb Blood Flow Metab*, vol. 13, pp. 5–14, Jan 1993.

[31] B. Biswal, F. Z. Yetkin, V. M. Haughton, and J. S. Hyde, "Functional connectivity in the motor cortex of resting human brain using echo-planar mri," *Magn Reson Med*, vol. 34, pp. 537–41, Oct 1995.

[32] M. J. Lowe, B. J. Mock, and J. A. Sorenson, "Functional connectivity in single and multislice echoplanar imaging using resting-state fluctuations," *Neuroimage*, vol. 7, pp. 119–32, Feb 1998.

[33] D. Cordes, V. M. Haughton, K. Arfanakis, J. D. Carew, P. A. Turski, C. H. Moritz, M. A. Quigley, and M. E. Meyerand, "Frequencies contributing to functional connectivity in the cerebral cortex in "resting-state" data," *AJNR Am J Neuroradiol*, vol. 22, pp. 1326–33, Aug 2001.

[34] M. Hampson, B. S. Peterson, P. Skudlarski, J. C. Gatenby, and J. C. Gore, "Detection of functional connectivity using temporal correlations in mr images," *Hum Brain Mapp*, vol. 15, pp. 247–62, Apr 2002.

[35] S. Ogawa, T. M. Lee, A. R. Kay, and D. W. Tank, "Brain magnetic resonance imaging with contrast dependent on blood oxygenation," *Proc Natl Acad Sci U S A*, vol. 87, pp. 9868–72, Dec 1990.

[36] P. Jezzard, P. M. Matthews, and S. M. Smith, "Functional mri an introduction to methods," 2001.

[37] S. C. Strother, "Evaluating fmri preprocessing pipelines," *IEEE Eng Med Biol Mag*, vol. 25, pp. 27–41, Mar-Apr 2006.

[38] P. A. Bandettini, A. Jesmanowicz, E. C. Wong, and J. S. Hyde, "Processing strategies for time-course data sets in functional mri of the human brain," *Magn Reson Med*, vol. 30, pp. 161–73, Aug 1993.

[39] K. J. Friston, A. P. Holmes, K. J. Worsley, J. P. Poline, C. D. F. R., and S. J. Frackowiak, "Statistical parametric maps in functional imaging: A general linear approach," *Human Brain Mapping*, vol. 2, no. 4, pp. 189–210, 1994.

[40] D. B. Rowe and R. G. Hoffmann, "Multivariate statistical analysis in fmri," *IEEE Eng Med Biol Mag*, vol. 25, pp. 60–4, Mar-Apr 2006.

[41] P. Jezzard, D. LeBihan, D. Cuenod, L. Pannier, Prinster,A, and Turner,R, "An investigation of the contribution of physiologic noise in human functional mri studies at 1.5 tesla and 4 tesla.," 1992.

[42] R. M. Weisskoff, Baker,J, Belliveay,J, T. L. Davis, K. K. Kwong, M. S. Cohen, and B. R. Rosen, "Power spectrum analysis of functionally-weighed mr data: What's in the noise?," 1992.

[43] S. J. Peltier, T. A. Polk, and D. C. Noll, "Detecting low-frequency functional connectivity in fmri using a self-organizing map (som) algorithm," *Hum Brain Mapp*, vol. 20, pp. 220–6, Dec 2003.

[44] C. F. Beckmann, M. DeLuca, J. T. Devlin, and S. M. Smith, "Investigations into resting-state connectivity using independent component analysis," *Philos Trans R Soc Lond B Biol Sci*, vol. 360, pp. 1001–13, May 29 2005.

[45] P. Bellec, V. Perlbarg, S. Jbabdi, M. Pelegrini-Issac, J. L. Anton, J. Doyon, and H. Benali, "Identification of large-scale networks in the brain using fmri," *Neuroimage*, vol. 29, pp. 1231–43, Feb 15 2006.

[46] J. S. Damoiseaux, S. A. Rombouts, F. Barkhof, P. Scheltens, C. J. Stam, S. M. Smith, and C. F. Beckmann, "Consistent resting-state networks across healthy subjects," *Proc Natl Acad Sci U S A*, vol. 103, pp. 13848–53, Sep 12 2006.

[47] S. J. Peltier and D. C. Noll, "T(2)(*) dependence of low frequency functional connectivity," *Neuroimage*, vol. 16, pp. 985–92, Aug 2002.

[48] S. J. Peltier, C. Kerssens, S. B. Hamann, P. S. Sebel, M. Byas-Smith, and X. Hu, "Functional connectivity changes with concentration of sevoflurane anesthesia," *Neuroreport*, vol. 16, pp. 285–8, Feb 28 2005.

[49] A. B. Waites, A. Stanislavsky, D. F. Abbott, and G. D. Jackson, "Effect of prior cognitive state on resting state networks measured with functional connectivity," *Hum Brain Mapp*, vol. 24, pp. 59–68, Jan 2005.

[50] S. J. Peltier, S. M. LaConte, D. M. Niyazov, J. Z. Liu, V. Sahgal, G. H. Yue, and X. P. Hu, "Reductions in interhemispheric motor cortex functional connectivity after muscle fatigue," *Brain Res*, vol. 1057, pp. 10–6, Sep 28 2005.

[51] T. E. Lund, "fcmri–mapping functional connectivity or correlating cardiac-induced noise?," *Magn Reson Med*, vol. 46, pp. 628–9, Sep 2001.

[52] T. H. Le and X. Hu, "Retrospective estimation and correction of physiological artifacts in fmri by direct extraction of physiological activity from mr data," *Magn Reson Med*, vol. 35, pp. 290–8, Mar 1996.

[53] G. H. Glover, T. Q. Li, and D. Ress, "Image-based method for retrospective correction of physiological motion effects in fmri: Retroicor," *Magn Reson Med*, vol. 44, pp. 162–7, Jul 2000.

[54] K. J. Friston, S. Williams, R. Howard, R. S. Frackowiak, and R. Turner, "Movement-related effects in fmri time-series," *Magn Reson Med*, vol. 35, pp. 346–55, Mar 1996.

[55] M. D. Fox, A. Z. Snyder, J. L. Vincent, M. Corbetta, D. C. V. Essen, and M. E. Raichle, "The human brain is intrinsically organized into dynamic, anticorrelated functional networks.," *Proc Natl Acad Sci U S A*, vol. 102, pp. 9673–9678, Jul 2005.

[56] D. Cordes, J. Carew, H. Eghbalnia, E. Meyerand, M. Quigley, K. Arfanakis, A. Assadi, P. A. Turski, and V. Haugthon, "Resting-state functional connectivity study using independent component analysis, 1706," in *Proceedings of the 7th Scientific Meeting of the International Society for Magnetic Resonance in Medicine, May 24-28, 1999, Philedelphia, Pennsylvania*, 1999.

[57] S. C. Strother, J. R. Anderson, K. A. Schaper, J. J. Sidtis, J. S. Liow, R. P. Woods, and D. A. Rottenberg, "Principal component analysis and the scaled subprofile model compared to intersubject averaging and statistical parametric mapping: I. "functional connectivity" of the human motor system studied with [15o]water pet.," *J Cereb Blood Flow Metab*, vol. 15, pp. 738–753, Sep 1995.

[58] A. R. McIntosh, F. L. Bookstein, J. V. Haxby, and C. L. Grady, "Spatial pattern analysis of functional brain images using partial least squares.," *Neuroimage*, vol. 3, pp. 143–157, Jun 1996.

[59] A. R. McIntosh, M. N. Rajah, and N. J. Lobaugh, "Functional connectivity of the medial temporal lobe relates to learning and awareness.," *J Neurosci*, vol. 23, pp. 6520–6528, Jul 2003.

[60] R. C. Craddock, S. Y. Masalovich, S. J. Peltier, X. P. Hu, and H. S. Mayberg, "Multivariate anlaysis of resting state fmri in major depression using seedpls," in *Proceedings of the 14th Scientific Meeting of the International Society for Magnetic Resonance in Medicine, May 6-12, 2006, Seattle, Washington*, 2006.

[61] K. A. Norman, S. M. Polyn, G. J. Detre, and J. V. Haxby, "Beyond mind-reading: multi-voxel pattern analysis of fmri data.," *Trends Cogn Sci*, vol. 10, pp. 424–430, Sep 2006.

[62] C. H. Y. Fu, J. Mourao-Miranda, S. G. Costafreda, A. Khanna, A. F. Marquand, S. C. R. Williams, and M. J. Brammer, "Pattern classification of sad facial processing: toward the development of neurobiological markers in depression.," *Biol Psychiatry*, vol. 63, pp. 656–662, Apr 2008.

[63] L. Zhang, D. Samaras, D. Tomasi, N. Volkow, and R. Goldstein, "Machine learning for clinical diagnosis from functional magnetic resonance imaging," in *Proc. IEEE Computer Society Conference on Computer Vision and Pattern Recognition CVPR 2005*, vol. 1, pp. 1211–1217, 20–25 June 2005.

[64] C. Z. Zhu, Y. F. Zang, M. Liang, L. X. Tian, Y. He, X. B. Li, M. Q. Sui, Y. F. Wang, and T. Z. Jiang, "Discriminative analysis of brain function at resting-state for attention-deficit/hyperactivity disorder.," *Med Image Comput Comput Assist Interv Int Conf Med Image Comput Comput Assist Interv*, vol. 8, no. Pt 2, pp. 468–475, 2005.

[65] Y. Fan, H. Rao, H. Hurt, J. Giannetta, M. Korczykowski, D. Shera, B. B. Avants, J. C. Gee, J. Wang, and D. Shen, "Multivariate examination of brain abnormality using both structural and functional mri.," *Neuroimage*, vol. 36, pp. 1189–1199, Jul 2007.

[66] I. Guyon and A. Elisseeff, "An introduction to variable and feature selection," *J. Mach. Learn. Res.*, vol. 3, pp. 1157–1182, 2003.

[67] V. N. Vapnik, *Statistical Learning Theory*. Wiley, 1998.

[68] C. J. C. Burges, "A tutorial on support vector machines for pattern recognition," *Data Min. Knowl. Discov.*, vol. 2, no. 2, pp. 121–167, 1998.

[69] B. Efron and R. J. Tibshirani, *An Introduction to the Bootstrap*. Chapman & Hall/CRC, May 1994.

[70] R. C. Elandt, "The folded normal distribution: Two methods of estimating parameters from moments," *Technometrics*, vol. 3, p. 551, Novermber 1961.

[71] K. A. Heberlein and X. Hu, "Simultaneous acquisition of gradient-echo and asymmetric spin-echo for single-shot z-shim: Z-saga," *Magn Reson Med*, vol. 51, pp. 212–6, Jan 2004.

[72] T. E. Lund, K. H. Madsen, K. Sidaros, W.-L. Luo, and T. E. Nichols, "Non-white noise in fmri: does modelling have an impact?," *Neuroimage*, vol. 29, pp. 54–66, Jan 2006.

[73] H. S. Mayberg, "Modulating dysfunctional limbic-cortical circuits in depression: towards development of brain-based algorithms for diagnosis and optimised treatment.," *Br Med Bull*, vol. 65, pp. 193–207, 2003.

[74] K. J. Friston, P. Rotshtein, J. J. Geng, P. Sterzer, and R. N. Henson, "A critique of functional localisers.," *Neuroimage*, vol. 30, pp. 1077–1087, May 2006.

[75] T. H. Le and X. Hu, "Methods for assessing accuracy and reliability in functional mri.," *NMR Biomed*, vol. 10, no. 4-5, pp. 160–164, 1997.

[76] S. C. Strother, J. Anderson, L. K. Hansen, U. Kjems, R. Kustra, J. Sidtis, S. Frutiger, S. Muley, S. LaConte, and D. Rottenberg, "The quantitative evaluation of functional neuroimaging experiments: the npairs data analysis framework," *Neuroimage.*, vol. 15, pp. 747–771, 04 2002.

[77] J. Talairach and P. Tournoux, *Co-planar stereotaxic atlas of the human brain. 3-Dimensional proportional system: an approach to cerebral imaging*. Thieme, 1988.

[78] K. Zilles and K. Amunts, "Receptor mapping: architecture of the human cerebral cortex," *Current Opinion in Neurology*, vol. 22, no. 4, pp. 331–339 10.1097/WCO.0b013e32832d95db, 2009.

[79] M. Beckmann, H. Johansen-Berg, and M. F. Rushworth, "Connectivity-based parcellation of human cingulate cortex and its relation to functional specialization," *J Neurosci*, vol. 29, pp. 1175–90, Jan 28 2009.

[80] D. S. Margulies, A. M. Kelly, L. Q. Uddin, B. B. Biswal, F. X. Castellanos, and M. P. Milham, "Mapping the functional connectivity of anterior cingulate cortex," *Neuroimage*, vol. 37, pp. 579–88, Aug 15 2007.

[81] Z. Wang, M. Fernández-Seara, D. C. Alsop, W.-C. Liu, J. F. Flax, A. A. Benasich, and J. A. Detre, "Assessment of functional development in normal infant brain using arterial spin labeled perfusion mri.," *Neuroimage*, vol. 39, pp. 973–978, Feb 2008.

[82] M. J. McKeown, S. Makeig, G. G. Brown, T. P. Jung, S. S. Kindermann, A. J. Bell, and T. J. Sejnowski, "Analysis of fmri data by blind separation into independent spatial components," *Hum Brain Mapp*, vol. 6, no. 3, pp. 160–88, 1998.

[83] M. van den Heuvel, R. Mandl, and H. H. Pol, "Normalized cut group clustering of resting-state fmri data," *PLoS One*, vol. 3, no. 4, p. e2001, 2008.

[84] A. Mezer, Y. Yovel, O. Pasternak, T. Gorfine, and Y. Assaf, "Cluster analysis of resting-state fmri time series," *Neuroimage*, vol. 45, pp. 1117–25, May 1 2009.

[85] C. Goutte, P. Toft, E. Rostrup, F. Nielsen, and L. K. Hansen, "On clustering fmri time series," *Neuroimage*, vol. 9, pp. 298–310, Mar 1999.

[86] A. G. He, L. H. Tan, Y. Tang, G. A. James, P. Wright, M. A. Eckert, P. T. Fox, and Y. Liu, "Modulation of neural connectivity during tongue movement and reading," *Hum Brain Mapp*, vol. 18, pp. 222–32, Mar 2003.

[87] R. Patel, D. Borsook, and L. Becerra, "Modulation of resting state functional connectivity of the brain by naloxone infusion," *Brain Imaging and Behavior*, vol. 2, no. 1, pp. 11–20, 2008.

[88] A. L. Cohen, D. A. Fair, N. U. Dosenbach, F. M. Miezin, D. Dierker, D. C. Van Essen, B. L. Schlaggar, and S. E. Petersen, "Defining functional areas in individual human brains using resting functional connectivity mri," *Neuroimage*, vol. 41, pp. 45–57, May 15 2008.

[89] M. D. Fox, A. Z. Snyder, J. L. Vincent, M. Corbetta, D. C. V. Essen, and M. E. Raichle, "The human brain is intrinsically organized into dynamic, anticorrelated functional networks.," *Proc Natl Acad Sci U S A*, vol. 102, pp. 9673–9678, Jul 2005.

[90] U. von Luxburg, "A tutorial on spectral clustering," *Statistics and Computing*, vol. 17, no. 4, pp. 395–416, 2007.

[91] J. Shi and J. Malik, "Normalized cuts and image segmentation," *IEEE Transactions on Pattern Analysis and Machine Intelligence*, vol. 22, no. 8, pp. 888–905, 2000.

[92] S. Yu and J. Shi, "Multiclass spectral clustering," IEEE Computer Society, 2003.

[93] N. Palomero-Gallagher, B. A. Vogt, A. Schleicher, H. S. Mayberg, and K. Zilles, "Receptor architecture of human cingulate cortex: evaluation of the four-region neurobiological model," *Hum Brain Mapp*, vol. 30, pp. 2336–55, Aug 2009.

[94] T. A. Yousry, U. D. Schmid, H. Alkadhi, D. Schmidt, A. Peraud, A. Buettner, and P. Winkler, "Localization of the motor hand area to a knob on the precentral gyrus. a new landmark," *Brain*, vol. 120 (Pt 1), pp. 141–57, Jan 1997.

[95] S. T. Grafton, J. C. Mazziotta, R. P. Woods, and M. E. Phelps, "Human functional anatomy of visually guided finger movements," *Brain*, vol. 115 (Pt 2), pp. 565–87, Apr 1992.

[96] S. M. Rao, D. L. Harrington, K. Y. Haaland, J. A. Bobholz, R. W. Cox, and J. R. Binder, "Distributed neural systems underlying the timing of movements," *J Neurosci*, vol. 17, pp. 5528–35, Jul 15 1997.

[97] V. H. Scholz, A. W. Flaherty, E. Kraft, J. R. Keltner, K. K. Kwong, Y. I. Chen, B. R. Rosen, and B. G. Jenkins, "Laterality, somatotopy and reproducibility of the basal ganglia and motor cortex during motor tasks," *Brain Res*, vol. 879, pp. 204–15, Oct 6 2000.

[98] P. A. Lewis, H. D. Critchley, P. Rotshtein, and R. J. Dolan, "Neural correlates of processing valence and arousal in affective words," *Cereb Cortex*, vol. 17, pp. 742–8, Mar 2007.

[99] D. A. Seminowicz, H. S. Mayberg, A. R. McIntosh, K. Goldapple, S. Kennedy, Z. Segal, and S. Rafi-Tari, "Limbic-frontal circuitry in major depression: a path modeling metanalysis.," *Neuroimage*, vol. 22, pp. 409–418, May 2004.

[100] A. Anand, Y. Li, Y. Wang, J. Wu, S. Gao, L. Bukhari, V. P. Mathews, A. Kalnin, and M. J. Lowe, "Activity and connectivity of brain mood regulating circuit in depression: a functional magnetic resonance study.," *Biol Psychiatry*, vol. 57, pp. 1079–1088, May 2005.

[101] A. Anand, Y. Li, Y. Wang, M. J. Lowe, and M. Dzemidzic, "Resting state corticolimbic connectivity abnormalities in unmedicated bipolar disorder and unipolar depression.," *Psychiatry Res*, vol. 171, pp. 189–198, Mar 2009.

[102] A. Anand, Y. Li, Y. Wang, J. Wu, S. Gao, L. Bukhari, V. P. Mathews, A. Kalnin, and M. J. Lowe, "Antidepressant effect on connectivity of the mood-regulating circuit: an fmri study.," *Neuropsychopharmacology*, vol. 30, pp. 1334–1344, Jul 2005.

[103] X. Wang, R. Hutchinson, and T. M. Mitchell, "Training fmri classifiers to detect cognitive states across multiple human subjects," in *In NIPS03*, pp. 709–716, 2003.

[104] L. Baldaçara, J. G. F. Borgio, A. L. T. de Lacerda, and A. P. Jackowski, "Cerebellum and psychiatric disorders.," *Rev Bras Psiquiatr*, vol. 30, pp. 281–289, Sep 2008.

[105] A. Anand, Y. Li, Y. Wang, K. Gardner, and M. J. Lowe, "Reciprocal effects of antidepressant treatment on activity and connectivity of the mood regulating circuit: an fmri study.," *J Neuropsychiatry Clin Neurosci*, vol. 19, no. 3, pp. 274–282, 2007.